IEEE Access
Multidisciplinary | Rapid Review | Open Access Journal

Received 25 May 2024, accepted 8 June 2024, date of publication 20 June 2024, date of current version 27 June 2024.

Digital Object Identifier 10.1109/ACCESS.2024.3416874

RESEARCH ARTICLE

Sampling Period Analysis for Deterministic and Stochastic Controllers: An Algorithmic Tool for Performance Optimization

MARYSON DA SILVA ARAÚJO AND ANTONIO DA SILVA SILVEIRA
Laboratory of Control and Systems, Federal University of Pará, Belém 66075-110, Brazil

Corresponding author: Maryson da S. Araújo (maryson@ufpa.br)

This work was supported by the Pro-Dean of Research and Graduate Studies of the Federal University of Pará (PROPESP/UFPA), by means of the Qualified Publication Support Program (PAPQ).

ABSTRACT The leading contribution of this article is to describe the analysis of the sampling period in deterministic and stochastic pole-assignment-based digital controllers, by proposing an analysis tool that considers the Nyquist-Shannon frequency and quantitative performance indices to guide the sampling period selection, optimizing the trade-off between closed-loop performance and sampling frequency smallness. In order to do so, the method employs discrete-time equivalent processes based on other five benchmark continuous-time, system identification of ARX and ARMAX reduced-order models of these processes, stochastic pole-assignment design based on Generalized Minimum Variance control, which inherits the loop-shape from a deterministic Reference Signal Tracking control, as well as performance indexes are obtained and evaluated to assess the most adequate choices for the sampling period among several options with different trade-off outcomes. The simulation results validate the importance of the developed analysis tool, showing how sensitive the performance of the controlled processes is to the sampling period, especially when subjected to stochastic disturbances which normally affect most control systems. Nevertheless, some papers do not even mention or empirically elect a value for the sampling period. Therefore, it is concluded that the developed tool can be extremely useful in predicting optimal outcomes regarding the trade-off between the sampling period and the closed-loop performance in computer-controlled systems.

INDEX TERMS Digital control systems, generalized minimum variance control, Nyquist-Shannon frequency, performance assessment, pole-assignment control, predictive control, sampling period analysis, sampling period assignment, system identification.

I. INTRODUCTION

The importance of digital control systems in control and automation is a fact because of its numerous advantages when compared to continuous-time control systems, such as control software upgrades, real-time prediction and adaptation, supervision and performance assessment with automatic tuning, and more, all running along and with the digital control algorithm, as the technological evolution leads to it [1] and [2]. In this context, much research has been carried out looking for the conversion of continuous-time control systems into discrete-time as shown in [3], [4], [5], [6], [7], and [8] while considering that the best discrete-time equivalent choice would be the best approximation of continuous-time systems [1], [8], [9], [10]. The sampling period is one of the parameters to be chosen in this conversion, considered an important issue [1], [2], [11] and it has been studied ever since [8], [12], [13], [14], [15], [16], [17], as it can be confirmed by the number of publications over the last two decades, depicted in Fig. 1, related to researches on sampled-data systems or sampling period analysis.

The sensitivity to the sampling period affects the system identification procedure (in the experimental modeling sense) of a discrete-time model of a continuous-time dynamic process, as studied by [3], which stated that a minimal

The associate editor coordinating the review of this manuscript and approving it for publication was Nasim Ullah.

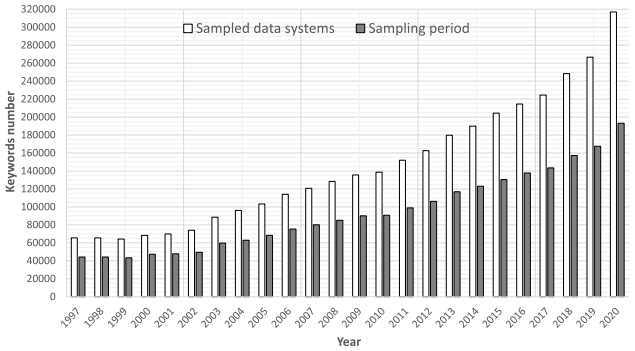

FIGURE 1. "Sampled-data system" and "sampling period" keywords on researches.

sampling period is not always the best choice and that there is an optimal one. In fact, an excessively short sampling period can cause control performance degradation in some continuous-time processes controlled via computers, as well as lose the advantages of digital control such as the reduction of actuator's state changes and control signal chattering [13].

A comparison among several sampling periods in digital control techniques has been reported in [4] and [5]. In the latter reference the sampling period was pointed as a key tuning parameter for self-tuning control algorithms, proposing a systematic sampling period selection based on the data. The approach of using the sampling period as another tuning parameter was also reported in [12], which could enhance stability and some of the specifications of the design problems through sampling period modifications.

How the choice of the sampling period affects the identification of nonlinear models, including their structure, estimated parameters, and quality, was investigated by [18], while [6] studied the effects of enlarging and decreasing the sampling period and the outcomes of such changes in the bandwidth of digital control systems from the theoretical and experimental viewpoints. He observed their influence on the closed-loop performance and stability, with further results on the stability analysis reported in his subsequent work [19].

Researchers in [17] also investigated the effects of increasing the sampling period. Using a water pressure control system, they observed performance degradation and potential instability. The significant influence of sampling period and other parameters on electric power systems have also been highlighted by [20], proposing a novel stability criterion based on Lyapunov's Stability Theory and Linear Matrix Inequality that incorporates both sampling period and network time-delay. The impact of increased sampling period on parameter estimation accuracy in a dual-mass DC electromechanical system was studied in [16]. They decomposed the phenomenological model's differential equation via Discrete Wavelet Transform and estimated parameters using four sampling periods. Their results demonstrated that the variation of the sampling period significantly influences models with lower parameter values but has less impact on those with higher values. Furthermore, reducing the sampling period improves the estimation method's accuracy. These studies emphasize the importance of considering sampling period in control system design to avoid performance degradation and instability.

Power system controllers, often designed in continuous-mode, face performance degradation or instability when discretized with large sampling periods during implementation, as noted by [21]. This is particularly challenging in wind turbine systems, where high penetration reduces inertia and necessitates faster load frequency control to handle contingencies such as sudden loss of generation. To analyze this paradox, [21] studied a discrete-mode load frequency control scheme considering a large sampling period. The results demonstrate that this scheme ensures stable operation and reduces the communication network burden significantly. Additionally, the controller design, based on a large exponential decay rate, provides a fast frequency response to alleviate the impact of reduced system inertia due to high wind power penetration.

Starting from the viewpoint of the real-time implementation of digital controllers in embedded systems, [7] explored the choice of the sampling period and its influence on the controller's transfer function from the perspective of the finite length of the word in digital control systems, considering both its impact on the controlled system's stability and settling time (lower bound) and the limitations of digital implementation accuracy (higher bound). For a practical implementation on microprocessor-based systems, [22] has selected an optimal sampling period for a specific linear time-invariant regulator. It was proposed a configurable optimization-based approach for guiding the selection of the sampling period. This approach allows users to specify the relative emphasis between achieving high closed-loop fidelity and ensuring ease of implementation. This configurable approach has the potential to simplify controller design for embedded systems while balancing performance and implementation constraints.

A systematic evaluation approach for choosing the sampling period in sampled-data control systems was proposed by [23]. Their optimization scheme, simultaneously considering low-frequency performance, medium-frequency stability margins, and high-frequency control activity, enabled significantly shorter sampling period, compared to existing rules of thumb. This was demonstrated with a pole placement controller for an integral plant with time-delay and a third-order system, especially when combined with an anti-aliasing filter and optimal pole placement. Similarly, [24] also focused on pole placement control but investigated instead a reference signal tracking (RST) controller designed specifically within the context of control/programming co-design, dependent on the sampling period. While this approach offers improved robustness to processor load variations and flexibility in work recovery time, the complexity of the RST synthesis procedure increases significantly with higher order plants due to the large number of polynomial parameters involved. These studies highlight the potential of optimization-based

approaches for selecting sampling periods while considering performance and implementation constraints.

In model predictive control, for example, aiming at time delay compensation the sampling period selection is directly related to the number of samples to be predicted (or the output prediction horizon), which can misguide the designer to a non-optimal sampling period in order to attend computational burden constraints, such as the selection of a longer sampling period in order to reduce the prediction horizon. In [14], the optimal generalized predictive control (GPC) was applied considering the sampling period selection as the first stage of the tuning procedure, and after that the control and prediction horizons were chosen, assuming the effects of the sampling period in GPC's optimality in a hybrid discrete plus continuous control-loop. They demonstrated that this approach can lead to a more effective control design. Moreover, the researchers highlight the intuitive nature and potential universality of this method, suggesting its applicability to other MPC algorithms beyond GPC. This study underscores the importance of carefully considering the sampling period's influence on control performance and computational demands in MPC frameworks. By prioritizing sampling period selection early in the tuning process, designers can potentially achieve more efficient and robust control strategies.

Thus, the optimality of digital control systems is strongly linked to the selection of the sampling period [25]. The research in [8] evaluated the impact of the sampling period over the control performance assessment of an optimal tuning technique based on the integral time absolute error (ITAE) criterion for continuous and discrete-time PI and PID controllers, which was also used by [25] to analyze the huge influence of three different sampling frequencies over the performance of the digital PID control of a voltage source inverter. Also, as [8] stated and common sense in the control systems literature suggests, the enlargement of the sampling period decreases the closed-loop performance. However, if it is true for all classes of systems or if it is the optimal approach, is still an open topic for investigation as depicted in recent published works shown as follows.

Study [26] analyzed the limits of poles and zeros in a system's discrete-time equivalents under zero-order-hold (ZOH) and generalized sampled-data hold approaches, investigating the behavior as the sampling period approaches zero. While this theoretically leads to perfect equivalence with the continuous-time system, it comes with limitations. Such approaches, despite recent and thinkable from an implementation perspective due to the availability of high-end microprocessors and memory modules, this might face the requirements of the distributed control systems scenario, which is strongly dependent on wired and wireless networked systems subject to variable time delays and packet loss, such that control system robustness might be more likely achievable under more flexible sampling period constraints, for example with possible real-time reconfigurations due to network capability degradation.

Looking into the problem of maximizing the sampling period, in [27] the design and implementation methods were proposed to achieve robust digital controllers applicable to a class of non-linear system subject to the maximum sampling period. This approach has a strong potential for emerging automation technologies and consolidated ones as well, such as in controller area networks (CAN) applied to electric drives and motors, which may impose severe time constraints in order to produce appropriate torques and velocities with maximum efficiency. For instance, [28] specifically explores finding the maximum allowable sampling period for controlling a complex vehicular plant (MIMO servomechanisms) using a CAN system. The communication delays inherent to CAN networks highlight the importance of carefully assessing the trade-off between sampling period and control design requirements.

Pushing the boundaries of sampling period selection, [29] used a very low sampling frequency (maximizing the sampling period) in a predictive control approach, demonstrating its feasibility in high-power applications. This opens doors for using such controllers in scenarios where power consumption or communication bandwidth are critical. On the other hand, [10] studied an automatic adaptive sampling time for an embedded networked control system in which the sampling time is continuously adapted to a proper value to maintain the controller performance, both in wired and wireless networks, producing the output response with control performance's criteria. Finally, [30] focused on PI control for first-order dynamic processes. They derived a critical sampling period based on PI gains, guaranteeing zero steady-state error as long as the chosen sampling period remains below this limit. This finding helps designers avoid sub-optimal control performance due to incorrect sampling period selection.

As aforementioned, the sampling period selection is often related to the optimization techniques. They are very common in control systems with bio-inspired algorithms, LMIs, artificial neural networks, fuzzy logic, MPC, GPC, LQG and LQR. In an optimization context [31] leverages a fuzzy model with a hybrid search and rescue (SAR) and adaptive neuro-fuzzy interface system (ANFIS) approach (SAR-ANFIS) to optimize charging scenarios for electric vehicles (EVs). This optimization minimizes costs while providing policymakers with tools for budgeting future EV loads. The proposed method allows for coordinating diverse charging scenarios and offers autonomy for EV owners, enabling cost-effective charging regardless of their situation. Similarly, [32] proposes an optimal strategy for industrial energy management based on evolutionary computing. This strategy characterizes different charging situations - stochastic, off-peak, peak, and electric power research institute - to achieve optimal vehicle-to-grid integration considering cost and demand. Simulations

demonstrate that the methodology can systematically charge and discharge PEVs while significantly reducing operational costs, emissions, as well as improving grid efficiency and security. Similar to the works discussed previously, [33] also employ optimization techniques for a control system application. They present a methodology for optimizing the combined capacity of a hybrid renewable power generation system and energy storage in a grid-connected microgrid. This approach maximizes the benefits of both renewable energy sources and diverse energy storage options. The proposed strategy focuses on four key objectives for microgrid operation: minimizing costs, reducing blackhouse gas (GHG) emissions, achieving a higher emission reduction benefit cost (ERBC), and enhancing reliability. To address the computational complexity of a combined optimization problem, they formulate and solve it in a piece-wise manner. Real-world data is used to validate the proposed methodology and the resulting optimal solution demonstrates economic benefit, improved reliability, and reduced GHG emissions compared to other potential configurations.

Both [34] and [35] propose optimization-based approaches to selecting sampling periods in control systems, offering flexibility in balancing performance and implementation constraints. Studies in [34] propose an optimization-based approach to selecting the sampling periods for classes of linear time-invariant (LTI) regulators in a cascaded multi-rate control structure, to account for practical implementation on numeric systems. Starting from the Shannon-Nyquist sampling theorem, in order to ensure asymptotic stability of the closed-loop system from the control theory viewpoint, a configurable optimization-based approach is solved with the mixed-integer artificial bee colony (MI-ABC) algorithm, for selecting the sampling periods by specifying the emphasis between closed-loop fidelity and ease of implementation. The solution was illustrated in two case studies: the construction of the proposed functionals and their practical implications. The method permits assessing percentage improvements for a set of desired metrics, which can be rounded up to an order of magnitude compared to classical recommended sampling rate values, while still maintaining acceptable performances in an industrial context.

Studies in [35] gathered a set of analyses and design tools to determine the sampling rate of 1DOF and 2DOF control structures using an optimization-based approach, along with an approach of deducing a WCET (worst-case execution time) for linear and time-invariant-based regulators through a formal language model which can be implemented in a rapid control prototyping (RCP) software tool. For the sampling rate selection, the classical Shannon-sampling theorem is replaced by an optimization problem that encompasses the trade-off between the fidelity of the controllers representation along with the fidelity of the resulting closed-loop systems, and the implementation difficulty of the controllers. The end-to-end DC motor case study emphasized the design of the controllers for the widely used benchmark system, by focusing also on the proposed framework.

Overall, these studies showcase the potential of optimization-based approaches for selecting sampling periods, balancing performance, implementation, and computational demands in various control system designs.

In [15] it was investigated the problem of sampling period assignment in the design of digital state feedback controllers for systems subject to time-varying sampling periods and uncertain delays. The system was controlled through a communication network, using the gain-scheduled linear quadratic controller designed through linear matrix inequalities, where the sampling period and the network-induced delay were bounded within a known interval. Numerical experiments illustrate the efficiency and the validity of such an approach.

The importance of considering the discrete-time nature of embedded controllers applied to dynamic continuous-time plants was investigated in [36]. From new conditions based on linear matrix inequalities (LMI) obtained from the Lyapunov-Krasovskii Functionals approach, a design technique was applied to linear sampled-data controllers, designed to stabilizing linear systems. The results were validated through simulations and experiments applied to a didactic plant, contrasting discrete (long sampling period of 4500 ms) and hypothetically-continuous (due to short sampling period of 2 ms) controllers, these being PID and LQR based. Such results confirmed the superiority of the sampled-data control over the continuous-time one, especially for large sampling periods.

Beyond the well-established system theory for periodic/equidistant/fixed sampling period, there are several other techniques to choose the sampling period, e.g., stochastic sampling period, non-periodic/aperiodic/non-uniform/asynchronous sampling period, multi-rate sampling period, and event-based sampling period. In the event-based alternative, the system is sampled when the output has changed by a specific amount rather than with the passing of time, resulting in many conceptual advantages as the control not being executed unless it is required [37], [38]. So, this approach is an important means for reducing the load of the digital communication networks that are used to implement feedback control, adapting the usage of all elements in controlling the loop to the current needs (resource-aware design) [39]. Looking at this, [40] used a simulation example to demonstrate the effectiveness of addressing the dynamic event triggered distributed state and unknown parameter estimation problem for discrete-time nonlinear systems that have known linear dynamics and unknown nonlinearities and are subject to deception attacks.

Also studying event-based control, [41] find the optimal event-triggered control strategy for a given performance index function, so that the system can track the ideal signal while minimizing the cost function. The adaptive dynamic programming (ADP) method and dynamic event-based mechanism are used to solve the optimal tracking problem of continuous-time boiler turbine systems. Simulation results effectively demonstrate the feasibility of the developed

method in this industrial-oriented system, leading to benefits such as lower energy consumption and faster response time through reducing the number of controller updates. While event-based control offers advantages, it presents additional computational challenges during implementation compared to sampled-data control and should therefore be used strategically.

The aforementioned studies reinforce the importance of assessing the selection of the sampling period in control system design. The general rules for selecting the periodic sampling period may depend on the parameters of the control problem (dominant time constant, transport time delay, inertia constants or loop-quality indicators such as settling time or rise time), the objective or reference model [8], [42], as well as the dependence on the continuous-time process or desired closed-loop bandwidth [43], [44]. However, several studies in the context of digital control systems do not even mention the value of this important parameter [45], [46], or when they do, they lack justification for the selected sampling period (e.g., in [47], [48], [49], [50], [51], [52], [53]).

Moreover, the general rules for periodic sampling period selection have been established under the assumption of deterministic classes of systems. When it turns to systems corrupted by process and measurement noises, the more the sampling period reduces, the more these noises may compromise the digital control loop sensitivity to high frequency disturbances. However, if the sampling period is increased, then the samples corrupted by the noise may be assumed as the true value of the discrete signal under consideration, increasing the regulation error that generates a counter-action by the controller that could lead to further increase of error due to the corrupted sample. Thus, such a problem is indeed reflected in both the controlled output signal and the control signal, since the feedback loop brings the stochastic uncertainties into the control-loop.

When Karl J. Åström introduced the stochastic approach to control techniques by means of the self-tuning minimum variance regulator [54], the gap between the deterministic and stochastic control methods and their practical implementation was reduced [55] since, theoretically, it was possible to design the optimal deadbeat regulator to a particular discrete-time system corrupted by stochastic uncertainties. Even if the sampling period was increased up to a certain theoretically-accepted value, a maximum-likelihood-based predictor was used to obtain the predicted mean value of the corrupted (by noise) controlled output variable. However, such control technique does not explicitly takes into account the sampling period in order to verify other possible optimal outcomes. So, the importance of the sampling period selection becomes even more crucial when stochastic disturbances join the digital control system closed-loop analysis [11], [56].

In this present work the main contribution is focused on the development of a sampling period analysis tool, henceforth addressed as the SPA tool. The aim is to assist the control system designers in selecting the optimal sampling period to achieve a suitable trade-off between control system efficiency and the smallness of the sampling period, which is well known to significantly influence digital controller's performance and system identification by recursive parametric estimation techniques.

To evaluate the sampling period selection in the context of deterministic and stochastic digital control, the RST control and the Generalized Minimum Variance (GMV) control are employed, respectively. It is emphasized that the tuning of the GMV controller (GMVC) can be derived from a deterministic one adding the solution of the Diophantine equation related to the stochastic process model, completing the GMVC design. So the GMVC can inherit the desired closed-loop behavior (loop-shape) from any RST controller designed by the pole-assignment procedure, which leads to the generalization to the Stochastic Augmentation in [55] and [57], also known as the GMV recursive pole-assignment [58], [59], [60]. Such a procedure allows the compatible performance assessment of how the deterministic and the stochastic controls are affected by the changes in the sampling period with each closed-loop simulation, since a similar desired closed-loop specification is maintained.

This controller design approach offers several novelties. The sampling period becomes a tuning parameter for both deterministic and stochastic pole-placement controllers, applicable to linear process models of any order. It also considers energy/computational resources and design specifications. Furthermore, in the stochastic case (augmentation), it allows tuning of GMVC's pseudo-output filters even with non-minimal order specifications, unlike [50]. However, there are limitations. The design struggles with systems containing multiple discrete-time delays and might not converge for very large order process models due to potential numerical issues with Sylvester matrix inversion, required for both controller design. Hence, another difficulty is the desired controller representation in RST format (structure), which must result in a valid Sylvester matrix. If this is not possible, then there will be no solution for the controllers' design, derailing this synthesis for some controllers, like PID structures and some process models.

Therefore, this paper aims at proposing an analysis tool, the SPA, to assist in the selection of the sampling period by means of the performance assessment of deterministic and stochastic controllers via numerical simulations. The baseline relates to the indexes derived to analyze and guide the sampling period selection in terms of the most appropriate choice among several others employed and evaluated using the proposed methodological analysis.

Beyond this introductory section, this paper is structured as an overview of the key theories contained in each required procedure used by the analysis tool (discretization, system identification, RST and GMV control design, and performance criteria), simulation setups, qualitative and quantitative simulation results, and conclusions.

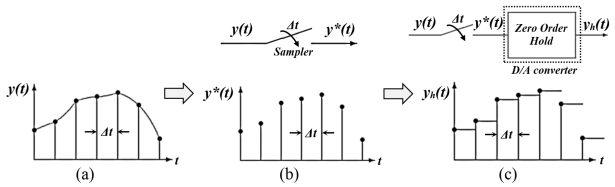

FIGURE 2. Sampling process in the control systems.

II. A REVIEW OF THEORIES EMPLOYED IN THE SAMPLING PERIOD ANALYSIS TOOL

This section aims at clarifying the primary theories employed in developing the proposed analysis tool, facilitating understanding of how to determine the most appropriate sampling period for controlling a discrete-time equivalent model of a linear continuous-time process.

A. SAMPLED-DATA CONTROL SYSTEMS

A sampled-data control system performs discrete control every time the analog-to-digital (A/D) converter (ADC) obtains a new sample from the controlled system output, and it calculates a single control value to update the digital-to-analog (D/A) converter (DAC), holding this value until the next control calculation occurs after a new output sample is fed back to the controller. The time interval between each sample is called sampling period, T_s, and it has the following relation to the sampling frequency or sampling rate, $f_s = \frac{1}{T_s}$ [1]. While a continuous-time system has infinite values for time and amplitude, a discrete-time system works only at predetermined instants. A digital system has finite values for both time and amplitude, with the ZOH transform representing an ideal DAC that holds the data from a digital system between T_s instants [2]. This process is illustrated in the simplified diagram shown in Fig. 2.

B. NYQUIST-SHANNON FREQUENCY

In sampled-data control, the time interval at which the controller periodically reads from and writes on the A/D and D/A converters must be chosen. This choice can be short or long, and the Nyquist-Shannon Sampling Theorem – the minimum sampling frequency (f_s') for perfect reconstruction of a continuous-time signal is twice the desired maximum frequency (f_B) – defines a minimum sampling rate ($f_s' \geq 2f_B$), or a maximum sampling period ($T_s' \leq \frac{T_B}{2}$) to be used by discrete-time systems [11], [42]. However, it does not determine the minimum T_s or a more suitable one [3], [7], [8], [14], [23], [36], [61].

In this present work, a solution based on Algorithm 1 is proposed and utilized to obtain the so-called fundamental Nyquist-Shannon frequency (f_{NS}') for five continuous-time benchmark processes. This frequency is identical to their cutoff frequency (f_B) and is defined as follows:

$$f_{NS} \triangleq \frac{f_s}{2} \therefore f_s = f_s' = 2f_B \Longrightarrow f_{NS} = f_{NS}' = f_B, \qquad (1)$$

where f_{NS} is the Nyquist frequency for each f_s.

Algorithm 1 Example for Nyquist-Shannon Frequency Calculation

$\vec{Mag} \leftarrow$ *process frequency response gains*;
$ne \leftarrow$ *elements in* $\vec{Mag}$;
for $kd \leftarrow ne$ **to** 1 **do**
  if $\vec{Mag}(kd) \leq \left(\vec{Mag}(1) - 3\right)$ **then**
    $kb \leftarrow kd$;
    break the repeat loop "for";
  end if
end for
$\omega_B \leftarrow \omega(kb)$; # Cutoff frequency [rad/s] at -3dB
$f_B \leftarrow \omega_B(kb)/(2\pi)$; # Cutoff frequency [Hz] at -3dB
$f_{NS}' \leftarrow f_B$; # Fundamental Nyquist-Shannon frequency
$T_{NS}' \leftarrow (f_{NS}')^{-1}$; # Fundamental Nyquist-Shannon period

TABLE 1. Continuous-time benchmark processes analysed on SPA.

Parameter	Process transfer function
$n = 3$	$G_{p1}(s) = \frac{1}{(s+1)^n}$
$\alpha = 0.1$	$G_{p2}(s) = \frac{1}{\prod_{n=0}^{3}(1+\alpha^n s)}$
$\alpha = 0.2$	$G_{p3}(s) = \frac{(1-\alpha s)}{(1+s)^3}$
–	$G_{p4}(s) = \frac{100}{(s+10)^2}\left[\frac{1}{s+1} + \frac{1}{s+0.05}\right]$
$\omega_0 = 10$, $\zeta = 0.1$	$G_{p5}(s) = \frac{\omega_0^2}{(s+1)(s^2+2\zeta\omega_0 s+\omega_0^2)}$

The Algorithm 1 computes the f_{NS}' values based on the process frequency response, when its gain decay 3 *dB* from its DC frequency value, i.e. the cutoff frequency. The f_{NS}' is the foundation of the proposed SPA tool which in turn is based on the Nyquist criterion, employing multiples of f_{NS}' (MSNF), so-named Nyquist-Shannon sampling harmonics, i.e. $f_s = mf_s'$ or $T_s = (mf_s')^{-1}$, $m \in \mathbb{Z}_+^*$.

C. SOME CONTINUOUS-TIME BENCHMARK PROCESSES

Whereas the SPA tool requires deterministic and stochastic models for each T_s, it was decided to use high-order continuous-time benchmark processes. This decision was made in order to identify reduced-order discrete-time approximations to simulate the plant-model-mismatch and to consider unmodeled dynamics as stochastic uncertainties, which were obtained based on the residuals of the system identification procedure. Thus, five models proposed by [62], [63] were employed to evaluate PID controllers. These models are widespread for evaluating other control techniques. Details of these processes are provided in Table 1, and their identified versions are presented in Section II-D.

D. BENCHMARK CONTINUOUS-TIME SYSTEMS DISCRETIZATION AND IDENTIFICATION

The system identification is the term that has been used mainly for the procedure of measuring signals at the input and output of a dynamic system and building a model to

represent it for control system design [64]. In the present paper the ARX (AutoRegressive with eXogenous input) and ARMAX (AutoRegressive Moving Average with eXogenous input) second-order models are obtained via Recursive Least Squares (RLS) and Extended RLS (ERLS) [42], [64], [65], respectively, by processing cause and effect data from the unity step response experiment applied to the ZOH discrete-time equivalents of the continuous-time benchmark processes shown in Table 1.

Since all benchmark processes used were of order greater than two, then both ARX and ARMAX models derived will eventually have unmodeled dynamics in order to assess plant-model-mismatch problems within a controlled simulation environment. Thus, the modeled process noise of the ARX and ARMAX models were obtained based on this plant-model-mismatch using the ARX and ARMAX models validation data, i.e., the error signal between the benchmark process output and the estimated output.

Each sampling period value used in the identification procedure, within the interval of one to forty times the fundamental Nyquist-Shannon frequency, i.e., $(40f'_{NS})^{-1} \leq T_s \leq (f'_{NS})^{-1}$, originates a deterministic and a stochastic model (cf. Fig. 3, where $a_0 = c_0 = 1$ for all of them). This wide interval was chosen to cope with the various range-values suggested by the scientific community [1], [2], [4], [11], [42], [43], [44]. Also, concerning the use of the step response to excite the processes, this is justified since it is a commonly adopted test signal to observe the transient response for system identification [62], in which many industrial processes can be analyzed from [11] and [42]. Added, the multiple correlation coefficient (R^2) was employed to quantify the quality of the models [65]:

$$R^2 = 1 - \frac{\sum_{k=1}^{N}[y(k) - \hat{y}(k)]^2}{\sum_{k=1}^{N}\left[y(k) - \mu_y\right]^2}, \tag{2}$$

where N is the number of registered samples of $y(k)$ with mean μ_y, used to obtain the model's estimated output $\hat{y}(k)$. Many practical applications in system identification for control system design consider a sufficient R^2 index in the range of $0.8 \leq R^2 \leq 1$, with the best value being $R^2 = 1$, which would depict an exact match between the output and its estimate [65].

E. DETERMINISTIC AND STOCHASTIC CONTROL DESIGN

This subsection approaches the deterministic and stochastic controllers design and explains how they were used in the SPA tool.

1) RST POLE ASSIGNMENT CONTROLLER

A single degree-of-freedom (DOF) controller, like the PID controller, can fail when more complex dynamic processes need to be controlled [66]. Thus, a more sophisticated 2DOF controller, like the RST (Reference Signal Tracking), could be used in order to ensure stability, disturbance rejection, optimization within safety limits, as well as robustness [53], [66].

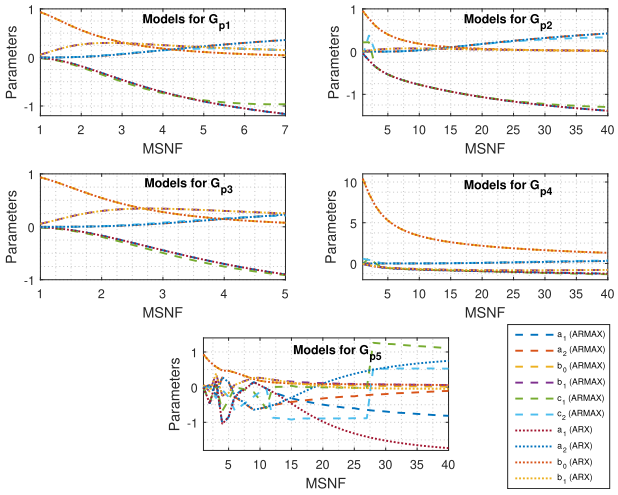

FIGURE 3. ARMAX and ARX models regarding MSNF values under analysis.

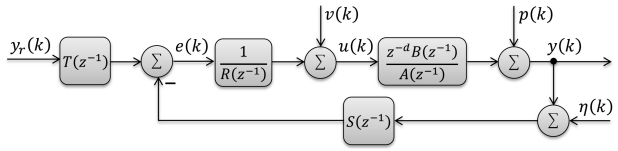

FIGURE 4. Canonical RST topology with measurement noise – $\eta(k)$ – and disturbances – $v(k)$ and $p(k)$.

The canonical polynomial structure of the RST controller (cf. Fig. 4) can be designed using a technique that involves the imposition of different dynamics on the plant by pole placement of the closed-loop poles of a continuous or discrete-time system, allowing it to fulfill the requirements of regulatory and tracking control, independently [67]. For that, two polynomials must be calibrated to satisfy a desired closed-loop performance. In addition, a third one filters the reference signal and can be calculated in a way to ensure performance in steady state [42].

In this context, a 2DOF pole assignment controller, like the RST, continues to be widely applied by the scientific community, e.g. in the process industry [51], [52], [67], [68], in robotics [51], in unmanned aerial vehicles (UAV) [53], [69], [70], in medicine [71], in optimal control algorithms [52], [67], [72] and hybrid systems [67], [70], in power systems [47], [48], [55], [73], in robust control [51], [52], [67], [68], [69], [70], [72], among others.

In Fig. 4 it is shown the block diagram of the canonical RST topology.

Whereas $p(k) = C[z^{-1}]\xi(k)$ with $C[z^{-1}] = 1$ in the control-loop at Fig. 4, an ARX model is defined by [64],

$$A[z^{-1}]y(k) = z^{-d}B[z^{-1}]u(k) + \xi(k), \tag{3}$$

where $A[z^{-1}]$, $B[z^{-1}]$ and $C[z^{-1}]$ are polynomials in z^{-1}, the backward shift operator domain, such that a function

TABLE 2. Polynomials' degree of incremental and positional RST controller.

Incremental RST	Positional RST
$n_r = n_a$	$n_r = n_a - 1$
$n_s = n_b + d - 1$	$n_s = n_b + d - 1$
$n_t = 0$	$n_t = 0$
$n_h \leq n_a + n_b + d - 1$	$n_h \leq n_a + n_b + d - 1$

$X[z^{-1}] = x_0 + x_1 z^{-1} + x_2 z^{-2} + \cdots + x_{n_x} z^{-n_x}$ with $n_x = degX[z^{-1}]$ and satisfying $z^{-m} y(k) \triangleq y(k-m)$ [42]. The process transport time delay plus the A/D and D/A converters hold delay are accounted together into d, which is an integer value multiple of T_s; lastly, $y(k)$ is the process variable (output), $u(k)$ is the control signal and $\xi(k)$ is a zero mean Gaussian disturbance in the discrete-time domain, i.e., $k \in \mathbb{Z}_+$.

Henceforth, polynomials such as $X[z^{-1}]$ will also be addressed as X^z when a compact notation is required. So, A^z, B^z, R^z, S^z, T_R^z, P^z, Q^z, T_G^z, H^z, H_N^z, E^z, C^z and F^z are all polynomials defined in z^{-1} domain.

Observing the block diagram in Fig. 4, assuming $p(k) = \nu(k) = \eta(k) = 0$, the RST control law is as follows:

$$R^z u(k) = S^z y(k) - T_R^z y_r(k). \tag{4}$$

Substituting (4) into (3) originates the complementary sensitivity transfer function $S_{yr}(z^{-1})$,

$$H_{cl}(z^{-1}) = \frac{H_N^z}{H^z} = \frac{z^{-d} B^z T_R^z}{A^z R^z + z^{-d} B^z S^z} = \frac{y(k)}{y_r(k)}, \tag{5}$$

where $y_r(k)$ is the discrete-time reference signal.

Therefore, by choosing the roots of $H[z^{-1}]$ it is possible to determine $R[z^{-1}]$ and $S[z^{-1}]$ polynomial parameters. It is possible to assign a closed-loop desired dynamic for (5) [43] by finding a solution to the Diophantine equation,

$$H^z = A^z R^z + z^{-d} B^z S^z. \tag{6}$$

Assuming the plant's open-loop transfer function does not have common factors (zero and pole equality), then the polynomials in (6) are coprime ($A^z R^z + z^{-d} B^z S^z \neq 0$) [11] and the Diophantine equation order must obey the relations shown in Table 2. Thus, there is a strictly causal system and it implies that (6) has a unique solution [11].

In order to conclude the synthesis of $H_{cl}(z^{-1})$, one way to compute T_R^z is assuming $T_R^z = t_{r0} = H[1]/B[1]$ (for positional RST) and $T_R^z = t_{r0} = S[1]$ (for incremental RST) [66]. Considering the incremental form, (4) and (6) change to,

$$R^z \Delta u(k) = S^z y(k) - T_R^z y_r(k), \tag{7}$$

$$H^z = \Delta A^z R^z + z^{-d} B^z S^z, \tag{8}$$

respectively, where $\Delta = 1 - z^{-1}$ (discrete-time difference operator), creating an ARIX model with $\Delta A^z = 1 + \bar{a}_1 z^{-1} + \bar{a}_2 z^{-2} + \cdots + \bar{a}_{n_{\bar{a}}} z^{-n_{\bar{a}}}$.

In this paper it is employed both the Sylvester matrix [11], [66] and pole assignment into $H[z^{-1}]$ to compute the RST polynomials design for generalized discrete-time processes, i.e., for any n_a and n_b with $d = 1$, described in Section II-E3.

Note that it is possible to change the dynamics of (6) or (8) to a desired closed-loop one [43]. Here the poles were assigned as [42] and [66],

$$H^z = 1 + h_1 z^{-1} + h_2 z^{-2}, \tag{9}$$

where $h_1 = -2e^{-\zeta \omega_n T_s} cos(\omega_n T_s \sqrt{1-\zeta^2})$ and $h_2 = e^{-2\zeta \omega_n T_s}$. The parameters ω_n (undamped frequency) and ζ (damping factor) can be calculated aiming the desired control quality (settling time, maximum overshoot, rise time, peak time and so on). In addition, high-order pole assignment is also possible since it obeys the conditions shown in Table 2.

2) GMV CONTROL

The theory of stochastic control came to fill up the gap in control problems where uncertainties and disturbances are more likely represented in probabilistic terms [55]. The importance of such theory has been evidenced on researches about new control techniques and real applications, e.g., [45], [46], [48], [49], [55], [56], [57], [59], [74], [75], and [76].

The GMVC was first introduced by Clarke and Gawthrop in 1975 [77] and it is one of the simplest model predictive control (MPC) methods [47]. It is based on the Minimum Variance (MV) regulator [78] and its major difference in relation to deterministic controllers is that it employs an ARMAX model,

$$A[z^{-1}]y(k) = z^{-d} B[z^{-1}]u(k) + C[z^{-1}]\xi(k), \tag{10}$$

i.e., it includes both deterministic and stochastic parts in its description, as it can be seen by comparing (3) and (10). Notice, now $C[z^{-1}] \neq 1$ and it filters $\xi(k)$ which is a disturbance modeled as a stochastic process with zero mean ($\mu_\xi = 0$) and variance σ_ξ^2 [54]. Thus, a GMVC has the skills to distinguish between noise and disturbances – $\eta(k)$, $\nu(k)$ and $p(k) = C[z^{-1}]\xi(k)$, depicted in Fig. 4 – from deterministic cause-and-effect dynamics [55].

The GMVC has a generalized (pseudo) output [49], [50],

$$\phi(k+d) = P^z y(k+d) - T_G^z y_r(k+d) + Q^z u(k), \tag{11}$$

which should be minimized according to the performance index [49], [55],

$$J = \mathbb{E}[\phi^2(k+d)], \tag{12}$$

where $\mathbb{E}[\cdot]$ is the mathematical expectation, since J counts on the prediction (d-steps in the future) in order to be minimized by solving $\partial J / \partial u(k) = 0$.

While $y_r(k+d)$ may be known *a priori*, $y(k+d)$ and $\xi(k+d)$ are future information (non-mensurable) in (11). Thus, $y(k+d)$ will become known via estimation of (10) d-steps ahead by using the minimum variance predictor (MVP) [48], [49], [50], [55], [77] as,

$$\hat{y}(k+d|k) = \frac{B^z E^z}{C^z} u(k) + \frac{F^z}{C^z} y(k). \tag{13}$$

They accrue from the solution of a Diophantine equation [50],

$$P^z C^z = A^z E^z + z^{-d} F^z, \tag{14}$$

which arises from splitting $\xi(k+d)$ in present and future portions used for the MPV calculation. There is a single solution for (14) taking $n_e = d-1$ and $n_f = max[(n_p + n_c), (n_a + n_e)] - d$, according to [50], [77].

By substituting (13) into (11) and rearranging it in order to optimize (12), the GMV control law is given by [48] and [50]:

$$u(k) = \frac{C^z T_G^z y(k+d) - F^z y(k)}{B^z E^z + C^z Q^z}, \tag{15}$$

which ensures the minimum variance for $\phi(k+d)$ in steady-state [50]. Therefore, by substituting (15) into (10) with $\nu(k) = \eta(k) = 0$, it is obtained the complementary sensitivity $S_{yr}(z^{-1})$ and the sensitivity $S_{yp}(z^{-1})$ transfer functions [79],

$$y(k) = S_{yr}(z^{-1}) y_r(k) + S_{yp}(z^{-1}) p(k), \tag{16}$$

$$y(k) = \frac{B^z T_G^z}{A^z Q^z + B^z P^z} y_r(k) + \frac{B^z E^z + C^z Q^z}{A^z Q^z + B^z P^z} p(k). \tag{17}$$

In addition, by considering $p(k) = 0$, the closed-loop transfer function in the ARX model case can be described as

$$\frac{y(k)}{y_r(k)} = \frac{B[z^{-1}] T_G[z^{-1}]}{A[z^{-1}] Q[z^{-1}] + B[z^{-1}] P[z^{-1}]}. \tag{18}$$

Note that both (17) and (18) are not influenced by the time delay d as it occurs in the deterministic case shown in (5).

Just like the RST controller, the GMVC will use the incremental form by considering an ARIMAX model instead of the ARMAX shown in (10) [48]. Thus, the main design equations are rewritten to the incremental control form:

$$\Delta A^z y(k) = z^{-d} B^z \Delta u(k) + C^z \xi(k), \tag{19}$$

$$\phi(k+d) = P^z y(k+d) - T_G^z y_r(k+d) + Q^z \Delta u(k), \tag{20}$$

$$P^z C^z = \Delta A^z E^z + z^{-d} F^z, \tag{21}$$

$$n_f = max[(n_p + n_c), (n_{\bar{a}} + n_e)] - d, \tag{22}$$

$$\Delta u(k) = \frac{C^z T_G^z y(k+d) - F^z y(k)}{B^z E^z + C^z Q^z}, \tag{23}$$

$$u(k) = u(k-1) + \Delta u(k), \tag{24}$$

$$y(k) = \frac{(B^z T_G^z) y_r(k) + (B^z E^z + C^z Q^z) p(k)}{\Delta A^z Q^z + B^z P^z}. \tag{25}$$

3) GENERALIZED POLE ASSIGNMENT FOR GMV (GPAGMV)

The Stochastic Augmentation is a control design technique already employed in the recursive form, so-called GMVPAC (GMV with Pole Assignment Controller) and GMVDPAC (GMV with Dynamic PAC) [58], [59], [60], and non-recursive one [55].

It will be explained below the design of the so-called GPAGMV control. It generalizes the solution of GMV's Diophantine equation by employing the Bezout Identity generalized solution [11], [42] as well as an improvement for the Aryabhatta's equation solution [11], [54], allocating the RST's pole assignment into the GMV control design.

As previously seen, both GMV and RST control laws are respectively described by

$$R[z^{-1}] u(k) = T_R[z^{-1}] y_r(k) - S[z^{-1}] y(k), \tag{26}$$

$$Q[z^{-1}] u(k) = T_G[z^{-1}] y_r(k) - P[z^{-1}] y(k), \tag{27}$$

considering that GMV's generalized output is not in its predicted form and that there is a control signal that stabilizes the system (i.e., $\phi(\infty) \to 0$). Comparing (26) with (27) it is possible to tune the GMV's weighting polynomials with the RST loop-shape in the same manner as [55] presented for the PID controller, thus leading to

$$Q^z = R^z, \quad P^z = S^z, \; T_G^z = T_R^z. \tag{28}$$

According to (26)-(28), the GMV control can absorb the pole assignment from RST, but it is still necessary to solve (14) [48], [49], [50], which in turn will be able to minimize σ_ϕ^2, completing its optimal stochastic tuning.

In this paper, the generalized Diophantine from the RST control design is solved building the generalized Sylvester matrix shown in (30) [11] and choosing the desired pole assignment, $\vec{\rho}^T = [h_1, \ldots, h_{(n_r+n_s+1)}]$, from (9), obeying Table 2 with $\vec{x}^T = [r_1, \ldots, r_{n_r}, s_0, \ldots, s_{n_s}]$ and $\vec{\alpha}^T = [\bar{a}_1, \ldots, \bar{a}_{n_{\bar{a}}}]$. Thus, one way to represent such a generalized solution is [11],

$$\vec{x} = \mathbf{M}^{-1}(\vec{\rho} - \vec{\alpha}). \tag{29}$$

$$\mathbf{M} = \begin{bmatrix} \overbrace{1 & 0 & \ldots & 0}^{n_r} & \overbrace{b_0 & 0 & \ldots & 0}^{n_s+1} \\ \bar{a}_1 & 1 & \ddots & \vdots & b_1 & b_0 & \ddots & \vdots \\ \bar{a}_2 & \bar{a}_1 & \ddots & 1 & b_2 & b_1 & \ddots & b_0 \\ \vdots & \bar{a}_2 & \ddots & \bar{a}_1 & \vdots & b_2 & \ddots & b_1 \\ \bar{a}_{n_{\bar{a}}} & \vdots & \ddots & \bar{a}_2 & b_{n_b} & \vdots & \ddots & b_2 \\ 0 & \bar{a}_{n_{\bar{a}}} & \ddots & \vdots & 0 & b_{n_b} & \ddots & \vdots \\ \vdots & 0 & \ldots & \bar{a}_{n_{\bar{a}}} & 0 & 0 & \ldots & b_{n_b} \end{bmatrix} \tag{30}$$

In addition, the generalized pole assignment for GMV (GPAGMV) has to satisfy (28) jointly with the generalized solution for (21), according to Algorithm 2, based on Aryabhatta's equation full solution, in which $n_c \neq 0$.

So, in the generalized design both RST controller and GPAGMV were obtained in order to analyze the influence of the sampling period for both deterministic and stochastic controllers, respectively. The selection of these methods was mainly because the desired dynamics for the controlled processes resemble themselves even when the sampling period would changes.

F. THE SAMPLING PERIOD ANALYSIS TOOL

The developed SPA employs the steps at Algorithm 3. Notice that it applies the previous theories in order to get a dataset to be analyzed and achieve the most adequate sampling period,

Algorithm 2 Generalized Pole Assignment for GMV (GPAGMV)

Require: $\vec{\Delta A}$, $\vec{C}$;
$n_e \leftarrow d-1$; $n_p \leftarrow n_s$; $n_f \leftarrow max[(n_p+n_c),(n_{\vec{a}}+n_e)]-d$;
$\vec{As}(1:n_e+1+n_f+1,1) \leftarrow \vec{0}$;
$\vec{As}(2:2+n_{\vec{a}}+1,1) \leftarrow \vec{\Delta A}^T(2:n_{\vec{a}}+1,1)$;
$\mathbf{As}(:,1) \leftarrow \vec{As}$;
for $k \leftarrow 2$ **to** (n_e+1) **do**
  $\mathbf{As}(:,1:k) \leftarrow \left[\mathbf{As},\ permute\ \vec{As}\ one\ element\ ahead\right]$;
end for
$\vec{Cs}(1:n_e+1+n_f+1,1) \leftarrow \vec{0}$;
$\vec{Cs}(1:n_c+1,1) \leftarrow \vec{C}^T$;
$\mathbf{Cs}(:,1) \leftarrow \vec{Cs}$;
for $k \leftarrow 2$ **to** (n_s+1) **do**
  $\mathbf{Cs}(:,1:k) \leftarrow \left[\mathbf{Cs},\ permute\ \vec{Cs}\ one\ element\ ahead\right]$;
end for
$\vec{E}(1) \leftarrow s_0$;
for $k \leftarrow 2$ **to** (n_e+1+n_f+1) **do**
  if $(k \leq (n_e+1))$ **then**
    $\vec{E}(k) \leftarrow \vec{Cs}(k,:)\cdot\vec{S}^T - \vec{As}(k,1:length\ of\ \vec{E})\cdot\vec{E}^T$;
  else
    $\vec{F}(k-(n_e+1)) \leftarrow \vec{Cs}(k,:)\cdot\vec{S}^T - \vec{As}(k,1:length\ of\ \vec{E})\cdot\vec{E}^T$;
  end if
end for

or similarly, sampling frequency, for discrete-time control loops. Thus, by using this tool it is possible to optimize the control design regarding both the desired performance index and the sampling period, as it can be seen later in III.

Algorithm 3 SPA Algorithm's

1. Definition of a continuous-time process (LTI - Linear Time-Invariant System);
2. Define a T_s value, a multiple of the fundamental Nyquist-Shannon sampling period (T'_{NS}) determined for the process in the step "1";
3. Discretization of the continuous-time process for prior T_s;
4. Compute the step response for the process in step "3" and use its cause-effect data to identify reduced-order ARX and ARMAX models (they are independent of the noisy scenario);
5. Design the digital controllers for the identified models;
6. Simulations with both controllers subject to stochastic disturbance on the process variable;
7. Performance indexes calculation for both controllers with the current T_s and save results;
8. Elect a new T_s, a multiple of the f'_{NS} (MSNF) too, and less than the previous T_s used;
9. Perform steps "3" through "8" for the next T_s to be analyzed; and
10. Examine the numerical results in order to achieve the optimal trade-off between sampling period and control system performance.

G. INDEXES FOR PERFORMANCE EVALUATION

In control system applications it is important to satisfy certain desired performance specifications. Thus, it is necessary to quantify them like in [8], [47], [50], [56], [75], [80], and [81].

A performance index is a number that indicates the quality of the control system performance, which is considered optimal when that number is either minimized or maximized [82]. There are several indices used for this purpose, mainly to assess reference tracking, disturbance rejection and control signal energy, and the most widespread in the literature are ISE, IAE, ITAE and ITSE [66], [75], [80], [82], [83].

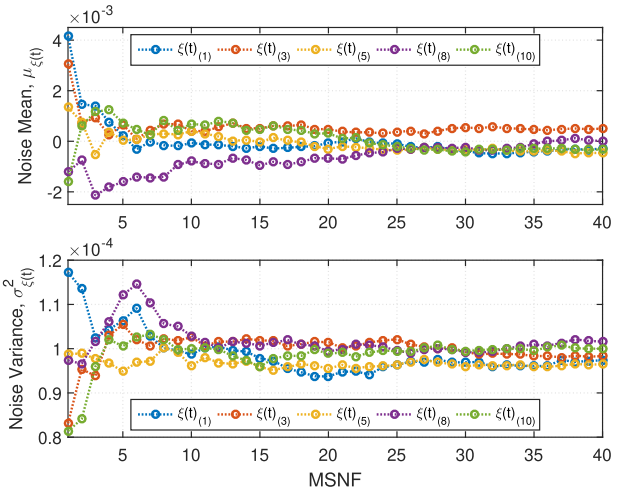

FIGURE 5. Mean and variance for five noise sequences regards each MSNF value. Such sequences was generated employing $\mu_\xi = 0$ and $\sigma^2_\xi = 10^{-4}$.

Here, the discrete-time indexes (sum) forms [50], [66] from the common performance integral indexes forms (e.g., IAE, ISE and ITAE) [80] and [82] were used. Those are based on the reference tracking error (SAE, SSE, STAE and STSE) and on the control signal (SACS, SSCS, STACS and STSCS), defined as follows:

$$SAE = \sum_{k=1}^{N} |e(k)|T_s, \quad SACS = \sum_{k=1}^{N} |u(k)|T_s,$$
$$STAE = \sum_{k=1}^{N} k|e(k)|T_s^2, \quad STACS = \sum_{k=1}^{N} k|u(k)|T_s^2,$$
$$SSE = \sum_{k=1}^{N} e^2(k)T_s, \quad SSCS = \sum_{k=1}^{N} u^2(k)T_s,$$
$$STSE = \sum_{k=1}^{N} ke^2(k)T_s^2, \quad STSCS = \sum_{k=1}^{N} ku^2(k)T_s^2.$$

The integral of time-weighted indexes (as *ITACS* and *ITSE*) are more suitable for transient analysis just like non time-weighted ones (like *IAE* and *ISCS*) are for steady-state [82]. So, these last indexes were utilized because the time-weighted ones tend to zero when T_{NS} decreases, since they employ the square of the sampling period, as it will be better emphasized in Section III. Furthermore, the IAE and IACS indexes are used because the error signal has an amplitude of less than 1 in steady-state, as suggested by [83].

III. SIMULATION RESULTS

This section shows the setups, the quantitative and the qualitative results, after employing the SPA tool for the simulations. Thus, the Algorithm 3 was applied to each process in Table 1, according to the parameters in Table 3, in order to get the dataset for the numerical analysis, from which the trade-off between the sampling period

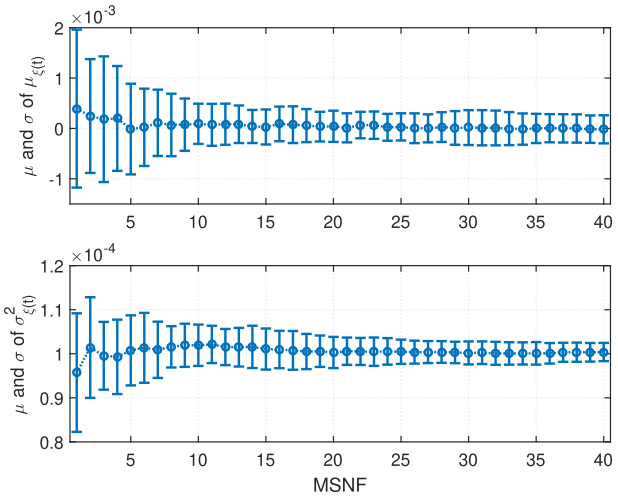

FIGURE 6. The trend of the noise mean and standard deviation according to MSNF values evaluated for twenty noise sequences applied to each MSNF.

TABLE 3. The SPA setups for simulation analysis.

Process	G_{p1}	G_{p2}	G_{p3}	G_{p4}	G_{p5}
Param.	$n=3$	$\alpha=0.1$	$\alpha=0.2$	–	$\omega_o=10$
f'_{NS} [Hz]	0.1702	0.3183	0.1638	0.0176	0.3656
T'_{NS} [s]	5.8754	3.1416	6.1054	56.7460	2.7349
MSNF	1:0.15:7	1:1:40	1:0.1:5	1:1:40	1:1:40*
t_{sim} [s]	170	91	177	1647	79
σ^2_ξ	10^{-3}	10^{-4}	10^{-3}	10^{-3}	10^{-5}
ω_n	0.5	2	0.5	0.7	1
ζ	0.8	0.8	0.8	0.8	0.8

smallness and control-loop performance was achieved for such controlled processes, as depicted in Table 4.

The following results were obtained using MATLAB 2015b 64-bit on Windows 7 Ultimate SP1 64-bit, running on a laptop with a Hewlett-Packard 1854 motherboard, an Intel Core i5-3230M processor, 8GB of DDR3 memory clocked at 1600MHz, and an SSD Sata-2.

A. SETUPS

Both controllers were evaluated concerning the noise disturbance, $\xi(t)$. In Fig. 5 it is shown two statistical features, mean (μ_ξ) and variance (σ^2_ξ), of just five of the twenty noise sequences applied to the simulations of the G_{p2} process for each MSNF. The MSNF is highlighted as a subscript of $\xi(t)$ since the number of samples in the noise sequence changes for every T_s value considered, affecting the two statistical features. Each process was evaluated according to Table 3 that shows the fundamental Nyquist-Shannon frequency and period obtained from the Algorithm 1.

In Table 3, it must be remarked that G_{p1} and G_{p3} were unable to allow a range for MSNF composed solely by integer values, since for higher values these systems became unstable in closed-loop with GMV. Then, for G_{p1}, MSNF ranged from 1 to 7 using steps of 0.15 (i.e., $1:0.15:7$) and for G_{p3}, from

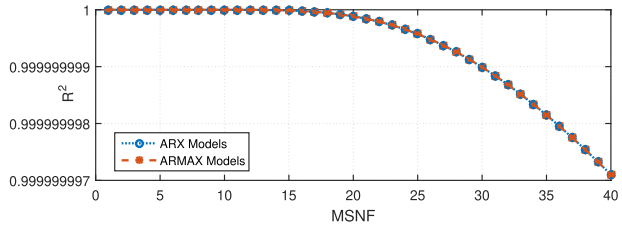

FIGURE 7. Multiple correlation coefficient for G_{p2} process identification regarding MSNF values.

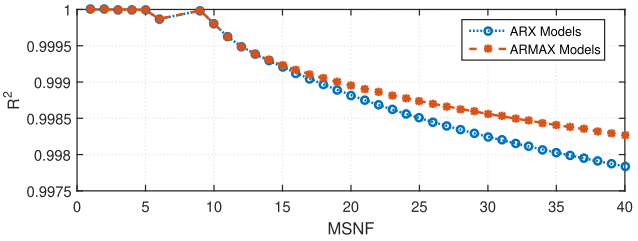

FIGURE 8. Multiple correlation coefficient for G_{p5} process identification regarding MSNF values.

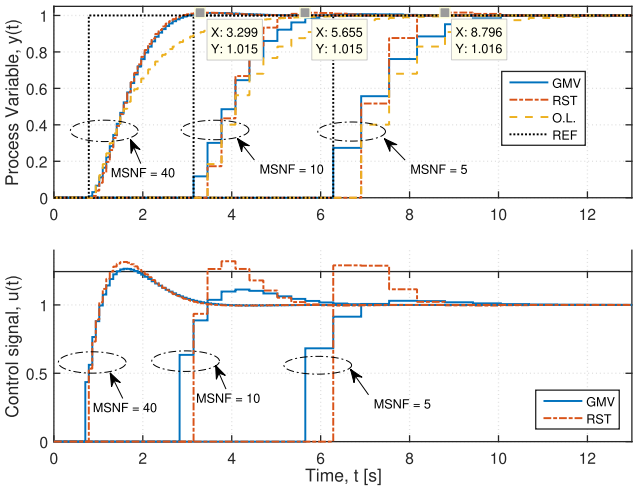

FIGURE 9. Comparison of the reference tracking performance of both controllers and the open-loop discrete-time response of the G_{p2} models for three MSNF (5, 10 and 40).

1 to 5 using steps of 0.1 (i.e., $1:0.1:5$). Another remark, regarding to G_{p5} and MSNF, is that except for MSNF $=\{7,\ 8\}$, G_{p5} could be stabilized with GMV control, thus in Table 3 the MSNF range was highlighted with "*". So, these facts already suggest a more cautious and systematic analysis when choosing the sampling period in GPAGMV control design, despite no such consideration has been found in previous GPAGMV studies, e.g., in [59], [60], and [55].

Notice that larger T_s (small MSNF values) affect more the μ_ξ and σ^2_ξ because there are few samples in the simulation regarding ones using narrower T_s (large MSNF). This behavior can be better seen in Fig. 6 looking at the aforesaid two statistical features.

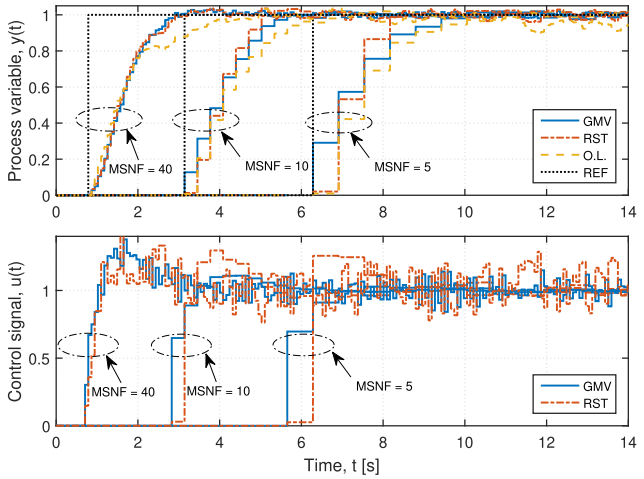

FIGURE 10. The reference tracking performance for both controllers and the open-loop discrete-time response for G_{p2} models when using three MSNF (5, 10 and 40) and adding noise in the process variable.

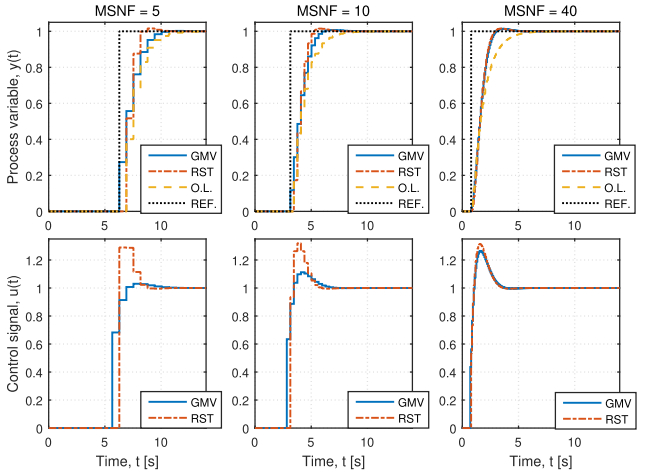

FIGURE 11. Comparison of the reference tracking performance of both controllers and the open-loop discrete-time response of the G_{p2} models for three MSNF (5, 10 and 40).

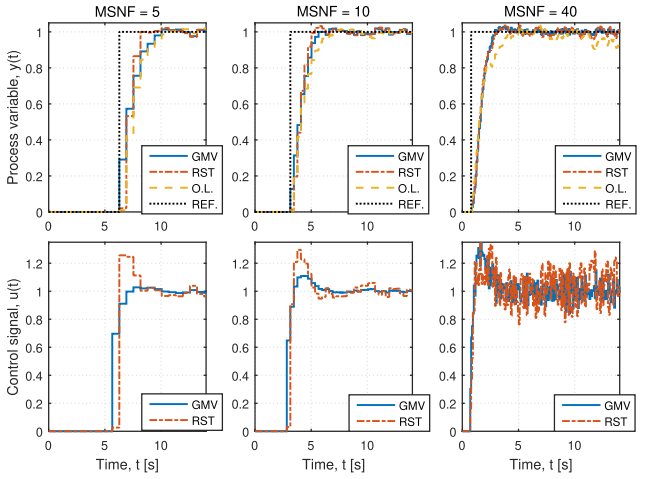

FIGURE 12. The reference tracking performance for both controllers and the open-loop discrete-time response for G_{p2} models when using three MSNF (5, 10 and 40) and noise affects the process variable.

Fig. 7 presents the G_{p2} process identification quality using second-order ARX and ARMAX models. Observe that the process was appropriately identified for control design purposes, concerning each T_s assessed, which is confirmed by the R^2 coefficients obtained [65], even using reduced-order models. This corroborates that it cannot be generalized that the lowest T_s is the best choice in system identification, as highlighted by [3]. Besides, the identification quality was slightly different for G_{p5}, as depicted in Fig. 8, but R^2 is suitable for practical applications, according to [65]. The best R^2 and trade-off sampling period were observed for larger T_s, as will be shown next.

A deeper analysis of the results is shown next, from sections III-B to III-D, related solely to the G_{p2} process for the sake of convenience. However, further results regarding the other processes will be highlighted in order to depict some results of more significance.

B. TRACKING PERFORMANCE FOR MSNF VALUES

In Fig. 9 it is shown the process variable and the control signal for both controllers as well as the open-loop response of the G_{p2} discrete-time process models for three MSNF values (5, 10 and 40).

Observe in Fig. 9 that all controlled responses are tracking the reference signal. This is also true for the white noise disturbance essay, as depicted in Fig. 10. The overshoot of 1.5%, which is bound to the desired ζ (shown in Table 3), was not achieved for the case where $MSNF = 5$ using the RST controller; thus resulting in a greater oscillation when the MSNF decreases, as mentioned in [2]. The GMV controller is more restrained overall, possibly because of its one step ahead prediction, as it can be seen by comparing its $u(t)$ signal to the one generated by the RST controller. Figures 11 and 12 improve the visualization of the control requirements for $y(t)$ and $u(t)$ for each mentioned MSNF.

In Fig. 13 it is shown the mean and standard deviation of the process variable variance (σ_y^2) and of the control signal variance (σ_u^2) when deterministic and stochastic controllers are operating in a noisy scenario.

Notice in Fig. 13 that both controllers increase the control signal variance when MSNF decreases, as highlighted by [4] and [11], regarding stochastic controllers. Besides, the RST starts building up a smooth raise when MSNF increases, degrading the disturbance rejection for the deterministic case. The same problem was observed for the G_{p5} process, as depicted in Fig. 14.

In GMVC, the mean value of the control and output variances tend to reduce as MSNF increase. The RST controller has achieved small mean variance values for G_{p2} and larger ones for G_{p5} with tendency to increase the control signal variance as f_s enlarges. This aspects are expected since the design of the minimum variance controller is better

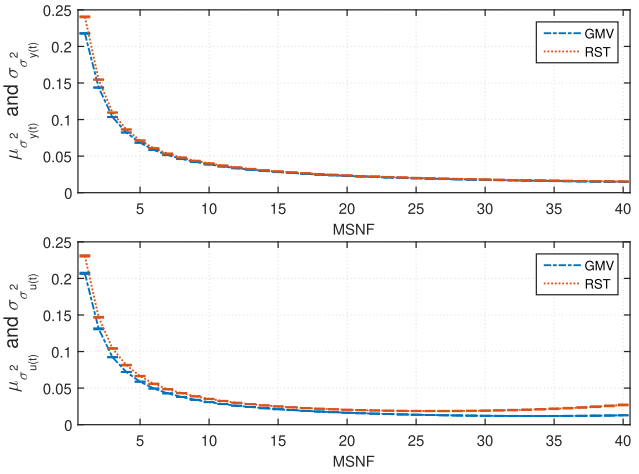

FIGURE 13. Comparison of mean and standard deviation of the variances (process variable and control signal) when applying both controllers to the G_{p2} models adding stochastic disturbances to the output.

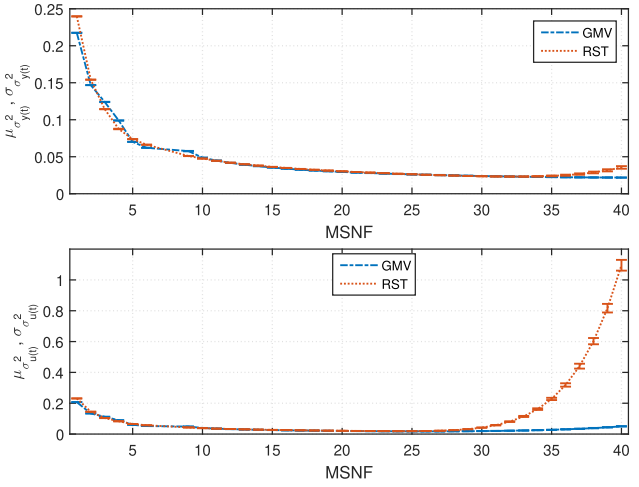

FIGURE 14. Comparison of mean and standard deviation of the variances (process variable and control signal) when applying both controllers to the G_{p5} models adding stochastic disturbances to the output.

to reject stochastic disturbances, attenuating these effects because of its stochastic approach.

The GMVC's mean variance values are fewer than or equal to those obtained by the deterministic controller, either for output or control signals. It is also worth mentioning that the difference between such values becomes greater as the MSNF is reduced.

C. PERFORMANCE INDEXES REGARDING MSNF AND STOCHASTIC DISTURBANCE

Since both controllers are tracking the reference signal for several T_s and noises, now it is evaluated how such scenario influences the SAE and SACS indexes when the GMV and RST controllers are applied to the processes under investigation while using the setups shown in Table 3.

In Fig. 15 there is the relation among the forenamed indexes regarding the control of the G_{p2} process models – one for each T_s or MSNF, applying twenty noise sequences

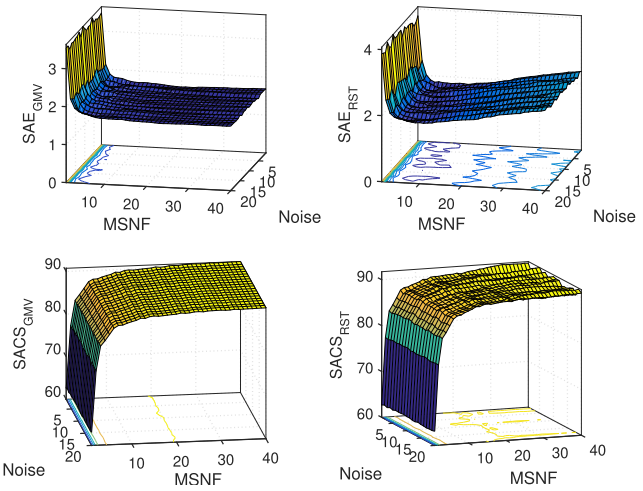

FIGURE 15. The SACS and SAE performances for G_{p2} models from both controllers for several MSNF and noises.

for each MSNF – whose variances are shown in Table 3. Thus, for instance, the left-superior created surface in Fig. 15 shows the relation between the four hundred computed index amplitudes (SAE for GMV controller) for each reference tracking response when each noise (stochastic disturbance) is applied to the process variable using every analysed MSNF. The other amplitude index surfaces are related to the RST controller reference tracking response and the SAE indexes for cited controllers' control signal, performing similar relations to originate the other three surfaces.

Observe in Fig. 15 that the SACS indexes are strongly attenuated while the SAE ones are highly increased when there is a MSNF decrease, either using GMV or RST, as considered in [2] and justified when [27] states that between samples, a sampled-data control system operates without feedback. Besides, each noise addition originates a slight variation in such indexes. In this stochastic scenario, notice that larger MSNF increases the RST's SAE while the GMV's one stays approximately constant, this being justified because of the stochastic approach of the GMV, whose design is performed to optimally reject stochastic disturbances – in this case for the MSNFs evaluated too. Also observe that the RST's SACS has slight oscillations when compared to GMV. From this behavior, consider it the application of methods that adapt both controllers in terms of T_s, for example, optimizing the control loop using it as a tuning parameter.

Figure 16 provides another way to see those variations and indexes in order to improve this assessment. Since some of such amplitudes are hidden in 3D graphics, this other viewpoint gets to show all of them, because each color on the colormap is related to each plane of amplitude, i.e., the amplitude slicing plane parallel to the MSNF-Noise plane is associated with each color. Thus, the attenuated variations in the aforesaid amplitudes result in a color regularity for distinct noises in the GMV controller, emphasizing again its stochastic approach [77]. On the other hand, reduced color

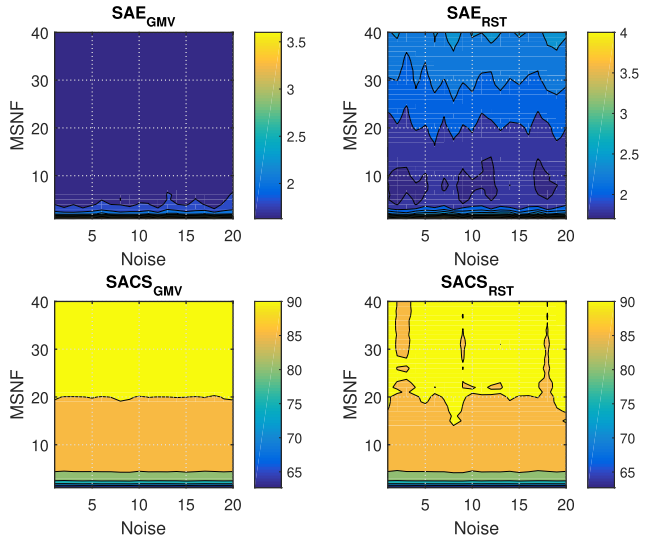

FIGURE 16. SACS and SAE performance indexes of G_{p2} models from both controllers for several MSNF and noises.

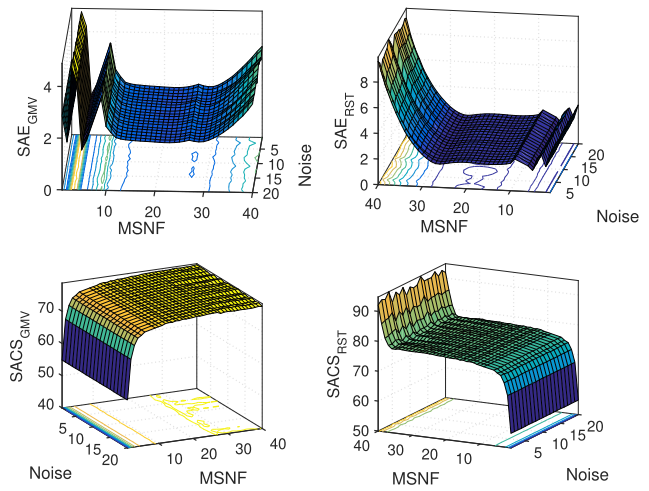

FIGURE 17. The SACS and SAE performances for G_{p5} models from both controllers for several MSNF and noises.

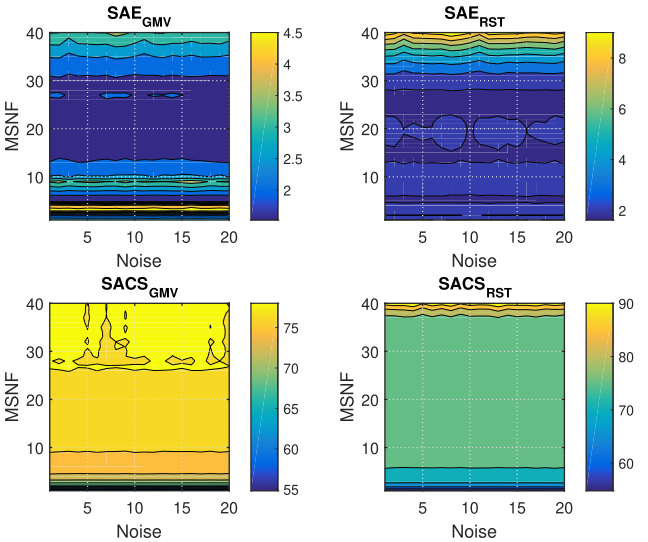

FIGURE 18. SACS and SAE performance indexes of the G_{p5} models from both controllers for several MSNF and noises.

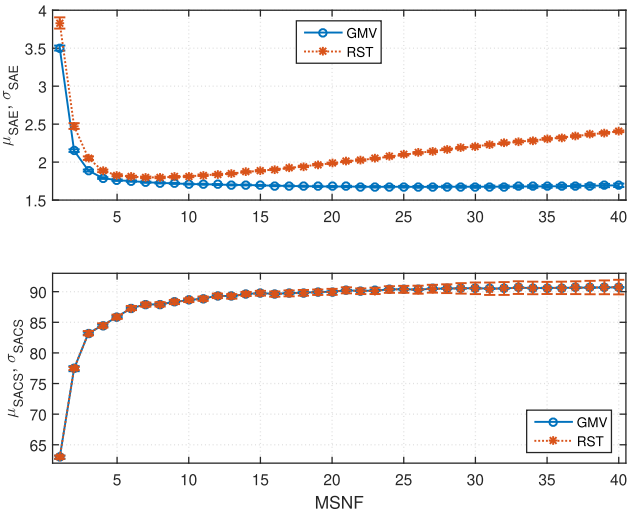

FIGURE 19. Mean and standard deviation of the SACS and the SAE performance indexes for G_{p2} models from both controllers for several MSNF and noises.

regularity is observed for the deterministic controller. The process G_{p5} was the unique exception to these comments, as depicted in Fig. 17 and Fig. 18.

The mean (μ) and standard deviation (σ) for both the SACS and SAE indexes are shown in Fig. 19, in order to statistically evaluate these indexes.

It was noticed in Fig. 19 that the noise sequences do not affect the SAE, neither for GMV nor RST controllers. However, the RST increases the SACS standard deviation (σ_{SACS}) when MSNF increases, i.e., this controller is more sensible to the noise, as expected: higher sampling frequencies results in more frequent control actions in deterministic control loops under a noisy scenario, once it has no stochastic control skills. Also, observe that the mean of SAE (μ_{SAE}) is enlarged in RST, while it does not change concerning the GMVC, as stated by [44] that faster sampling implies better disturbance rejection. Excepting the process G_{p5} (cf. Fig. 20), the GMV's μ_{SAE} is less or equal to the RST's one, where the last controller has higher deviation.

Figure 21 reveals the mean behavior of the absolute and square performance indexes for both the error and control signals regarding the MSNF.

For both digital controllers, by analyzing the absolute and the square performance indexes it is possible to elect a MSNF value that assures controlling the process, satisfying a better compromise between the error level and the control signals quality, i.e., the controlled processes do not have a minimum error but they also do not waste a large amount of energy in the control system [2], [36], [84]). Provided the mentioned trade-off can be employed for a controlled

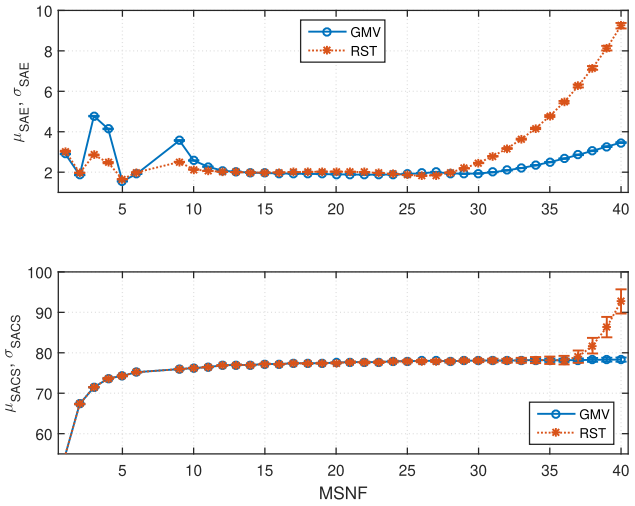

FIGURE 20. Mean and standard deviation of the SACS and the SAE performance indexes for G_{p5} models from both controllers for several MSNF and noises.

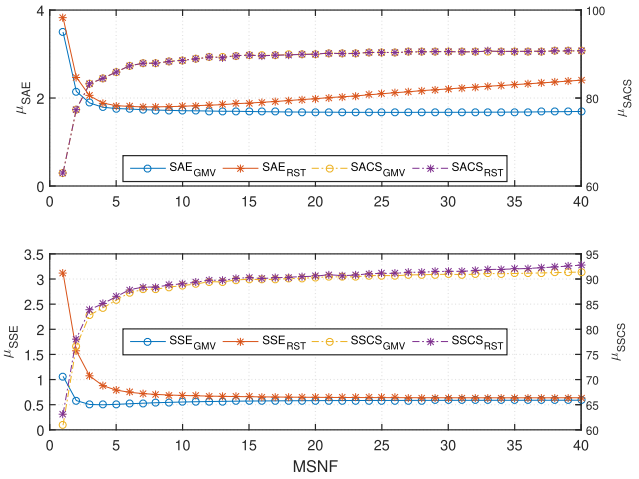

FIGURE 21. Mean of the absolute and the square performance indexes (control and error signals) when using both controllers and G_{p2} models.

process, the SPA allows the selection of a more suitable sampling period among the analyzed range, similar to [44] and [84] approaches, but with advantages highlighted next, e.g., the possibility of extending such choice for controlling high-order processes and minimizing the complexity of the mathematical approach for such selection in deterministic and stochastic linear discrete-time control systems.

Higher MSNF values increase the mean of the absolute error in the evaluated deterministic control, while in the stochastic one the mean is almost constant and, for the square index mean, it was observed a slight reduction in the control effort, consequently decreasing energy, computational effort, and network bandwidth resources, as highlighted in [84]. In both cases, the choice of large sampling frequency (MSNF) incurs almost no bonus for the system or, in the RST approach, there are even inferior performances, suggesting

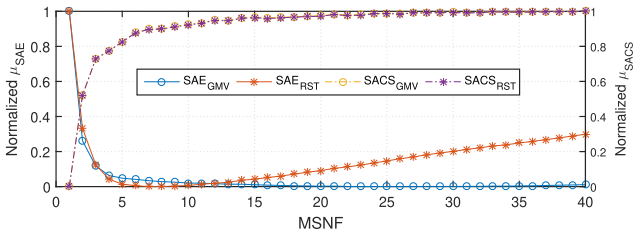

FIGURE 22. Comparison between normalized mean of the control and error performance indexes when both controllers are acting on G_{p2} models.

that higher sampling frequencies are always the worst choice. It achieved similar results when controlling the other benchmark processes shown in Table 3.

D. CHOOSING MSNF BASED ON THE TRADE-OFF PERFORMANCE INDEXES

From Fig. 21 results, it was noticeable that GMVC's squared performance indexes have sudden changes for small MSNF, but when MSNF is increased it is difficult to visualize the performance changes in order to choose the best compromise sampling period based on these squared indexes. Thus, the absolute ones (SACS and SAE) were chosen.

So, for the purpose of improving the visualization and comparison of the chosen indexes, Fig. 22 exhibits a normalized version for the mean of SAE and SACS performance indexes, regarding MSNF.

Based on the performance compromise, the selected sampling period is viewed and computed into the assessment range whose both SAE and SACS curves have simultaneous minimum value for the same MSNF. From Fig. 22, this value is $MSNF = 2$, i.e., $T_s = (2f'_{NS})^{-1} = 1.5708\ s$ or $f_s = 0.6366\ Hz$ for the GMV and $MSNF = 4$ for the RST. The other trade-offs for all the benchmark processes are shown in Table 4. Note that if the choice had been based on the curves shown in Fig. 21, the selected sampling period would be erroneous, since the μ_{SAE} and μ_{SACS} amplitudes were extremely different provided they were not normalized.

Based on the indexes trade-offs, the selected sampling period is then the minimum value of the normalized curve of the SACS's mean plus the minimum one for such SAE curve for every MSNF. Thereby, from Fig. 22, the compromise MSNF values are 2 and 4, for the GMV and the RST controllers, respectively. Such values were expected, since the sum (accumulation) of the error signal and the sum of the control signal are concurrent curves, related to MSNF (f_s), as shown in Fig. 23 and from values in Table 5, for instance. Besides, the sampling period directly influences the moment of control action, as stated in the control theory references and also shown in Fig. 23. Thus, there was the hypothesis of the compromise between these signals in relation to f_s and seen in Fig. 21, Fig. 22 and Fig. 24, a proof of concept from this work, since no references with such a contribution could be found previously.

TABLE 4. Compromise MSNF from SPA for all benchmark processes.

G_p	GMV			RST		
	MSNF	T_s [s]	f_s [Hz]	MSNF	T_s [s]	f_s [Hz]
G_{p1}	1.75	3.357	0.2978	1.75	3.357	0.2978
G_{p2}	2	1.5708	0.6366	4	0.7854	1.2732
G_{p3}	1.2	5.0878	0.1965	1.2	5.0878	0.1965
G_{p4}	3	18.9153	0.0528	32	1.7733	0.5639
G_{p5}	1	2.7349	0.3656	1	2.7349	0.3656

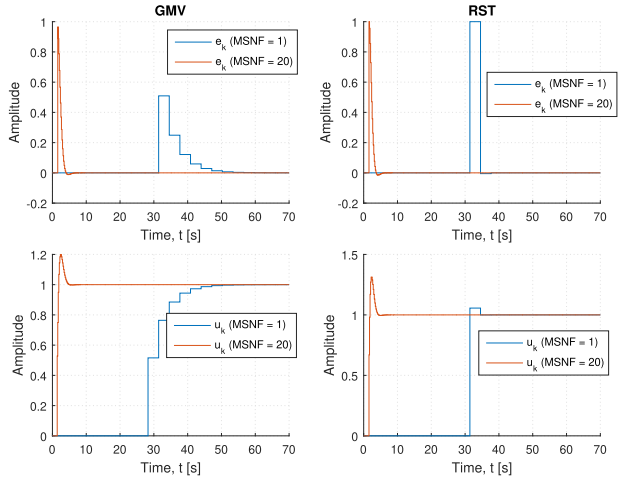

FIGURE 23. Error signal and control signal regarding two T_S (MSNF) for G_{p2} models.

TABLE 5. Accumulation of the error signal and the control signal regarding f_s.

G_p	MSNF	f_s [Hz]	GMV		RST	
			SACS	SAE	SACS	SAE
G_{p2}	1	0.31831	63.007	3.1258	63.007	3.1574
	20	6.3662	90.008	0.90615	90.008	0.91001
G_{p5}	1	0.36564	54.845	2.7952	54.845	2.8684
	20	7.3128	77.537	1.679	77.535	1.7072

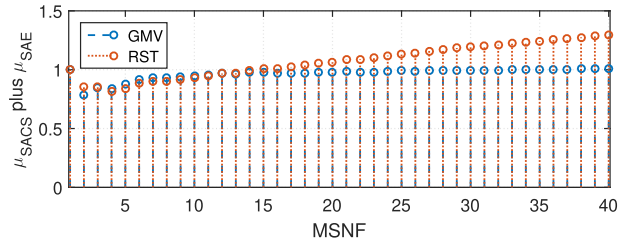

FIGURE 24. Curves summation of the absolute normalized mean of control and error performance indexes guiding to the best trade-off sampling period selection for the G_{p2} model.

The MSNF choice can be better observed and analyzed in Fig. 24, which shows the sum of the cited normalized curves, mainly because the other analyzed processes have many oscillations on such curves, interfering in this selection by mere visual inspection.

Overall, when observing Table 4 the stochastic controller can work with sampling frequencies lower than or equal to the deterministic one. Therefore, GMV has got the performance indexes trade-off with the lowest computational effort, possibly because of its optimal, predictive and stochastic characteristics. It is important to emphasize this result because a low f_s results in reduced computational burden, leaving more time to process data between successive data samples, to implement more sophisticated control algorithms possibilities and reducing network bandwidth resources requirements (reduces data load in feedback communication channels) [27].

It is worthy complementing that in all the studied cases – except for the deterministic control applied to G_{p4} – the trade-off was obtained for small sampling frequencies, as depicted in Table 4, with relation to the rule of thumb adopted in control systems like in [1], [2], [43], [44], and [85].

Finally, observe that the SPA tool places the T_s as a design parameter for both deterministic and stochastic pole assignment controllers, similar to what [12] and [13] presented in the deterministic approach. For that, it is enough to consult the normalized curve of the sum of the performance indexes, which shows the SACS and SAE evolution as a function of MSNF. Thus, the SPA creates an abacus to be consulted and starts the synthesis of new strategies in optimal digital control systems.

Besides what was, the SPA tool can also extend the assessments, for instance to high-order processes linear models, in addition to second-order ones evaluated here, as well as to other performance indexes, instead of SAE and SACS employed in the present paper.

IV. CONCLUSION

This paper addressed the development and application of an algorithmic technique for analyzing the periodic sampling period based on the Nyquist-Shannon criterion, the SPA, which uses the computational power to achieve the compromise (trade-off) sampling frequency for deterministic (RST) and stochastic (GMV) digital control systems designed by generalized pole assignment.

The GPAGMV design technique did not achieve a stable control system neither for all the assessed sampling frequencies, nor for all benchmark processes parameterization. Thus, not always the GMVC can absorb the RST pole assignment, having a dependency on the T_s. However, this fact has not been previously observed by any research on stochastic augmentation technique.

In the system identification procedure, the R^2 values decrease for narrow T_s. Thus, the SPA might open novel perspectives to guide researchers in the best selection of sampling periods for system identification, similarly to the works done in [3], [5], and [18]. Within the evaluated benchmark processes in this present paper, it was observed that lower sampling frequencies were generally more suitable, for both system identification and control.

From the error and control signals performance index values, it was possible to choose the f_s which sets a performance compromise for the controlled system using the deterministic or stochastic controllers. It was feasible to elect a MSNF value that assured controlling the processes satisfying the best trade-off for both control and error signals' quality, guaranteeing reduced energy consumption and satisfactory asymptotic reference tracking which can increase with larger values of f_s, mainly when using deterministic pole assignment controllers. Provided the SPA can be applied to a controlled process, the algorithm allows getting a more suitable T_s from an assessment range. Add to this the case where there are hardware limitations, such as in embedded control, the compromise as previously stated becomes imperative [44].

Regarding controllers, the large f_s increases the mean of the error by spending even more energy for deterministic control, while the stochastic one keeps this mean constant and slightly reduces the control effort. In both cases, the choice of large f_s incurs no bonus for the system or even decreases the performance. It was seen that the stochastic control approach had the most adequate performance compared to the deterministic one, especially in noisy scenarios. Besides, it was observed that the GMV's compromise sampling periods have values smaller or equal compared to RST ones, allowing the former to work with reduced computational effort.

The trade-off f_s was very close to the f'_{NS}, overall. Thus, the strategy of using GPAGMV indicates a way to improve even more the use of the embedded hardware, as long as slower sampling frequencies are allowed to the control system, which can cause problems mentioned in the literature as in [1], [2], [85]. The SPA tool places the T_s as a design parameter for pole placement deterministic and stochastic controllers, extending to the stochastic case the deterministic approaches of [12] and [13]. For that, it is enough to consult the sum of the normalized performance indexes curve, which shows the evolution of the SACS and SAE as the MSNF function, i.e., the SPA originates an abacus to be consulted.

The SPA allows the adoption of a trade-off f_s between performance and control effort, mitigating the computational burden, facilitating decision making without brilliant (despite complex) optimization calculations as in [44] and [84]. Furthermore, the generalized tuning of controllers with GPAGMV allows that the methodology could be extended to higher-order systems, something that has become unfeasible in the approach of [84] because it needed a complex analytical treatment.

This paper has shown that it is extremely important to test the f_s to be applied in deterministic and stochastic digital control systems. Such importance was shown per the quantitative approach employing the SPA, which uses the computer's processing power to create a numerical method to assist in the sampling period selection and substantiate this, rather than simply taking general rules for such selection/assignment or resorting to empiricism.

Future research aims at obtaining experimental results from the SPA tool applied to SISO didactic processes, via deterministic and/or stochastic control approaches, as well as at expanding it by incorporating other controllers and linear processes and developing the SPA in a state-space. Besides, such researches should culminate in a software for the scientific community, such as a MATLAB's toolbox, Scilab's ATOM, or a script/function tool for Python, for instance.

ACKNOWLEDGMENT

The authors thank the funding agency for its financial support.

REFERENCES

[1] G. F. Franklin, D. J. Powell, and M. L. Workman, *Digital Control of Dynamic Systems*. Upper Saddle River, NJ, USA: Adisson Wesley Longman Inc., 1998.
[2] K. J. Astrom and B. Wittenmark, *Computer-Controlled Systems: Theory and Design*. Upper Saddle River, NJ, USA: Prentice-Hall, 1997.
[3] A. Liff and J. Wolf, "On the optimum sampling rate for discrete-time modeling of continuous-time systems," *IEEE Trans. Autom. Control*, vol. AC-11, no. 2, pp. 288–290, Apr. 1966.
[4] B. Lennartson, "On the choice of controller and sampling period for linear stochastic control," in *Proc. 10th Triennial World Congr.*, 1987, vol. 26, no. 3, pp. 573–578.
[5] M. Kárný, "Estimation of sampling period for selftuners," *IFAC Proc. Volumes*, vol. 23, no. 8, pp. 285–290, Aug. 1990.
[6] P. Marango, "Observation on determining the sampling period in digital control," *IFAC Proc. Volumes*, vol. 31, no. 20, pp. 1043–1046, Jul. 1998.
[7] F. Dohnal and V. Rerucha, "Practical aspects of digital control system design–sampling period choice," *IFAC Proc. Volumes*, vol. 33, no. 1, pp. 219–223, Feb. 2000.
[8] M. Laskawski and M. Wcislik, "Sampling rate impact on the tuning of PID controller parameters," *Int. J. Electron. Telecommun.*, vol. 62, no. 1, pp. 43–48, Mar. 2016.
[9] V. Bobal, J. Bohm, J. Fessl, and J. Machacek, *Digital Self-tuning Controllers: Algorithms, Implementation and Applications*. Cham, Switzerland: Springer, 2005.
[10] N. Prempreechakun, S. Nuratch, and P. Boonpramuk, "Automatic sampling time adaptation for networked digital controller based-on embedded system," in *Proc. 1st Int. Symp. Instrum., Control, Artif. Intell., Robot.*, Jan. 2019, pp. 159–162.
[11] K. J. Astrom and B. Wittenmark, *Adaptive Control*, 2nd ed. New York, NY, USA: Dover, 2008.
[12] S. Dormido, I. Lopez-Rodriguez, J. L. Fdez-Marron, F. Morilla, and J. Aranda, "Design of digital control system using the sampling period as a compensator," in *Proc. 6th Medit. Electrotechnical Conf.*, 1991, pp. 812–815.
[13] I. Lopez, S. Dormido, and F. Morilla, "The sampling period as a control parameter," *IFAC Proc. Volumes*, vol. 27, no. 3, pp. 377–382, Jun. 1994.
[14] A. Wysocki and M. Ławrynczuk, "On choice of the sampling period and the horizons in generalized predictive control," in *Recent Advances in Automation, Robotics and Measuring Techniques*. Cham, Switzerland: Springer, 2014, pp. 329–339.
[15] E. S. Tognetti and T. R. Calliero, "Digital control and sampling period assignment of multiple plants in networked control systems," *IET Control Theory Appl.*, vol. 11, no. 17, pp. 3089–3096, Nov. 2017.
[16] M. Todorova and R. Parvanova, "Influence of the sampling period in the identification of a dual-mass DC electromechanical system using symlet wavelets," in *Proc. Int. Conf. Automatics Informat. (ICAI)*, Oct. 2020, pp. 1–5.
[17] T. Janus and B. Ulanicki, "Effects of sampling on stability and performance of electronically controlled pressure-reducing valves," *J. Water Resour. Planning Manage.*, vol. 147, no. 3, pp. 1–12, Mar. 2021.
[18] S. A. Billings and L. A. Aguirre, "Effects of the sampling time on the dynamics and identification of nonlinear models," *Int. J. Bifurcation Chaos*, vol. 5, no. 6, pp. 1541–1556, Dec. 1995.

[19] P. Marango, "Stability investigation of closed-loop system based on the sampling period," *IFAC Proc. Volumes*, vol. 32, no. 2, pp. 3742–3745, Jul. 1999.
[20] X.-C. Shangguan, C.-K. Zhang, Y. He, L. Jin, L. Jiang, J. W. Spencer, and M. Wu, "Robust load frequency control for power system considering transmission delay and sampling period," *IEEE Trans. Ind. Informat.*, vol. 17, no. 8, pp. 5292–5303, Aug. 2021.
[21] X. Shang-Guan, Y. He, C. Zhang, L. Jiang, J. W. Spencer, and M. Wu, "Sampled-data based discrete and fast load frequency control for power systems with wind power," *Appl. Energy*, vol. 259, Feb. 2020, Art. no. 114202.
[22] M. Suscă, V. Mihaly, D. Morar, and P. Dobra, "Quasi-optimal sampling time computation for LTI controllers," *IFAC-PapersOnLine*, vol. 55, no. 15, pp. 87–92, 2022.
[23] X. Peng, B. Lennartson, and C. Fransson, "On the choice of sampling period and robust pole placement," in *Proc. 15th Triennial World Congr.*, 2002, vol. 35, no. 1, pp. 97–102.
[24] D. Robert, O. Sename, and D. Simon, "Sampling period dependent RST controller used in control/scheduling co-design," *IFAC Proc. Volumes*, vol. 38, no. 1, pp. 225–230, 2005.
[25] M. Blachuta, R. Bieda, and R. Grygiel, "Sampling rate and performance of DC/AC inverters with digital PID control—A case study," *Energies*, vol. 14, no. 16, p. 5170, Aug. 2021.
[26] Y. Su, C. Zeng, D. Kang, X. Wang, and H. Wang, "Analytic study on the poles and zeros for mechanical plants," in *Proc. 3rd IEEE Int. Conf. Comput. Commun. (ICCC)*, Dec. 2017, pp. 2940–2944.
[27] H.-L. Choi and J. Hammer, "Sampled-data systems: Maximal sampling period," in *Proc. 57th Annu. Allerton Conf. Commun., Control, Comput. (Allerton)*, Sep. 2019, pp. 950–957.
[28] A. K. Singh and R. Potluri, "CAN-based networked path-tracking control of a 4WS4WD electric vehicle: Selection of sampling period and hardware-in-the-loop simulation," in *Proc. 20th Int. Conf. Distrib. Comput. Netw.*, Jan. 2019, pp. 1–10.
[29] J. A. Rohten, J. E. Muñoz, E. S. Pulido, J. J. Silva, F. A. Villarroel, and J. R. Espinoza, "Very low sampling frequency model predictive control for power converters in the medium and high-power range applications," *Energies*, vol. 14, no. 1, p. 199, Jan. 2021.
[30] S. Xu and C. Li, "Critical sampling period for sampled-data PI control systems," in *Proc. 41st Chin. Control Conf. (CCC)*, Jul. 2022, pp. 827–832.
[31] I. Ahmed, M. Rehan, A. Basit, M. Tufail, and K.-S. Hong, "Neuro-fuzzy and networks-based data driven model for multi-charging scenarios of plug-in-electric vehicles," *IEEE Access*, vol. 11, pp. 87150–87165, 2023.
[32] I. Ahmed, M. Rehan, A. Basit, M. Tufail, and K.-S. Hong, "A dynamic optimal scheduling strategy for multi-charging scenarios of plug-in-electric vehicles over a smart grid," *IEEE Access*, vol. 11, pp. 28992–29008, 2023.
[33] U. Akram, M. Khalid, and S. Shafiq, "An innovative hybrid wind-solar and battery-supercapacitor microgrid system—Development and optimization," *IEEE Access*, vol. 5, pp. 25897–25912, 2017.
[34] M. Suscă, V. Mihaly, and P. Dobra, "Sampling rate selection for multi-loop cascade control systems in an optimal manner," *IET Control Theory Appl.*, vol. 17, no. 8, pp. 1073–1087, May 2023.
[35] M. Suscă, V. Mihaly, D. Morar, and P. Dobra, "Sampling rate optimization and execution time analysis for two-degrees-of-freedom control systems," *Mathematics*, vol. 10, no. 19, p. 3449, Sep. 2022.
[36] A. N. D. Lopes, L. Arcese, K. Guelton, and A. Cherifi, "Sampled-data controller design with application to the quanser AERO 2-DOF helicopter," in *Proc. IEEE Int. Conf. Autom., Quality Test., Robot. (AQTR)*, May 2020, pp. 1–6.
[37] K. Johan Åström and B. Bernhardsson, "Comparison of periodic and event based sampling for first-order stochastic systems," *IFAC Proc. Volumes*, vol. 32, no. 2, pp. 5006–5011, Jul. 1999.
[38] K.-E. Årzén, "A simple event-based PID controller," *IFAC Proc. Volumes*, vol. 32, no. 2, pp. 8687–8692, Jul. 1999.
[39] M. Miskowicz, *Event-Based Control and Signal Processing*. Boca Raton, FL, USA: CRC Press, 2016.
[40] A. Basit, M. Tufail, M. Rehan, and C. K. Ahn, "Dynamic event-triggered approach for distributed state and parameter estimation over networks subjected to deception attacks," *IEEE Trans. Signal Inf. Process. Over Netw.*, vol. 9, no. 1, pp. 373–385, Jul. 2023.
[41] J. Zhang, D. Yang, H. Zhang, Y. Wang, and B. Zhou, "Dynamic event-based tracking control of boiler turbine systems with guaranteed performance," *IEEE Trans. Autom. Sci. Eng.*, pp. 1–11, 2004. [Online]. Available: https://ieeexplore.ieee.org/document/10185150, doi: 10.1109/TASE.2023.3294187.
[42] I. D. Landau and G. Zito, *Digital Control Systems: Design, Identification and Implementation*. London: Springer, 2006.
[43] I. D. Landau, "The R-S-T digital controller design and applications," *IFAC Proc. Volumes*, vol. 30, no. 6, pp. 23–33, May 1997.
[44] A. Cervin, M. Velasco, P. Marti, and A. Camacho, "Optimal online sampling period assignment: Theory and experiments," *IEEE Trans. Control Syst. Technol.*, vol. 19, no. 4, pp. 902–910, Jul. 2011.
[45] N. Mizuno, D. Kim, H. Sugiyama, and R. Fukatsu, "Application of adaptive minimum-variance control technique for cyclic production machine," *IFAC-PapersOnLine*, vol. 49, no. 13, pp. 146–151, 2016.
[46] N. Daou, H. F. Fassi, N. Ababssi, and Y. Djeghader, "Minimum variance control of active parallel filter for reduction of harmonics," *Revue Roumaine Des Sciences Techniques-Serie Electrotechnique Et Energetique*, vol. 64, no. 4, pp. 391–395, 2019.
[47] R. Trentini, R. Kutzner, and L. Hofmann, "State-space generalized minimum variance controller based PSS for damping of interarea modes," in *Proc. 18th Medit. Electrotechnical Conf. (MELECON)*, Apr. 2016, pp. 1–6.
[48] R. Trentini, A. Silveira, R. Kutzner, and L. Hofmann, "On the unrestricted horizon predictive control—A fully stochastic model-based predictive approach," in *Proc. Eur. Control Conf. (ECC)*, Jun. 2016, pp. 1322–1327.
[49] A. S. Silveira and A. A. R. Coelho, "Generalized minimum variance control state-space design," *IET Control Theory Applications*, vol. 5, no. 15, pp. 1709–1715, 2011.
[50] A. Silveira, R. Trentini, A. Coelho, R. Kutzner, and L. Hofmann, "Generalized minimum variance control under long-range prediction horizon setups," *ISA Trans.*, vol. 62, pp. 325–332, May 2016.
[51] B. Fernandez, P. J. Herrera, and J. A. Cerrada, "Robust digital control for autonomous skid-steered agricultural robots," *Comput. Electron. Agricult.*, vol. 153, pp. 94–101, Oct. 2018.
[52] P. Vongkoon and P. Liutanakul, "Frequency estimation improvement for single-phase phase-locked loop using digital RST controller," in *Proc. IEEE GTD Asia*, Sep. 2019, pp. 490–494.
[53] Z. A. Ali and X. Li, "Controlling of an under-actuated quadrotor UAV equipped with a manipulator," *IEEE Access*, vol. 8, pp. 34664–34674, 2020.
[54] K. J. Astrom, *Introduction to Stochastic Control Theory*. New York, NY, USA: Academic, 1970.
[55] R. Trentini, A. Silveira, M. T. Bartsch, R. Kutzner, and L. Hofmann, "On the design of stochastic RST controllers based on the generalized minimum variance," in *Proc. UKACC 11th Int. Conf. Control (CONTROL)*, Aug. 2016, pp. 1–6.
[56] L. Qida, T. Shubin, and Y. Yongkuan, "Performance evaluation of generalized minimum variance multi-disturbance control system," in *Proc. Chin. Control Decis. Conf. (CCDC)*, Jun. 2019, pp. 3286–3290.
[57] K. E. Lucas, D. J. Pagano, D. A. Plaza, D. A. Vaca-Benavides, and S. J. Ríos, "Stochastic control for DC–DC power converters: A generalized minimum variance control approach," *IFAC-PapersOnLine*, vol. 53, no. 2, pp. 13410–13417, 2020.
[58] M. A. Paz, E. Quintero-Marmol, R. Fernandez del Busto, E. Olguin, O. J. Santos, P. Ponce, and S. Garibo, "Improving stability and performance in a generalized minimum variance controller using dynamic pole assignment," in *Proc. 2nd Int. Conf. Electr. Electron. Eng.*, 2005, pp. 370–373.
[59] M. A. P. Ramos, E. Q.-M. Marquez, and R. F. del Busto, "Generalized minimum variance with pole assignment controller modified for practical applications," in *Proc. IEEE Int. Conf. Control Appl.*, Aug. 2004, pp. 1347–1352.
[60] M. A. P. Ramos, S. C. G. Esquivel, O. J. S. Sánchez, R. F. del Busto, J. F. B. de la Torre, J. L. G. Ramirez, and J. I. R. Martínez, "Generalized minimum variance controller with dynamic pole assignment to improve performance in industrial applications," in *Technological Developments in Networking, Education and Automation*. Cham, Switzerland: Springer, 2010, pp. 291–296.
[61] J. W. V. Dambros, M. Farenzena, and J. O. Trierweiler, "The effect of the sampling period on stiction detection methods," in *Proc. IIEEE Interface Conf. Control Appl.*, May 2004, vol. 50, no. 1, pp. 2848–2853.
[62] K. J. Astrom and T. Hagglund, *PID Controllers: Theory Design and Tuning*. Research Triangle Park, NC, USA: ISA, 1995.
[63] K. J. Åström and T. Hägglund, "Benchmark systems for PID control," *IFAC Proc. Volumes*, vol. 33, no. 4, pp. 165–166, Apr. 2000.
[64] L. Ljung and T. Soderstrom, *Theory and Practice of Recursive Identification*. Cambridge, MA, USA: MIT Press, 1983.

[65] A. A. R. Coelho and L. S. Coelho, *Identificacao De Sistemas Dinamicos*, 2nd ed. Florianopolis, Brazil: UFSC, 2015.
[66] A. A. R. Coelho, D. C. Jeronymo, and R. B. Araujo, *Sistemas Dinamicos: Controle Classico E Preditivo Discreto*. Florianopolis, Brazil: UFSC, 2019.
[67] R. Madiouni, S. Bouallègue, J. Haggège, and P. Siarry, "Robust RST control design based on multi-objective particle swarm optimization approach," *Int. J. Control, Autom. Syst.*, vol. 14, no. 6, pp. 1607–1617, Dec. 2016.
[68] J. Lu, Y. Bo, and J. Wang, "Research on high precision tracking of piezoelectric fast steering mirror," in *Proc. IEEE 16th Int. Conf. Netw., Sens. Control (ICNSC)*, May 2019, pp. 180–185.
[69] D. Stefanoiu, A. Stoica, C. Constantinescu, E. M. Cimpoesu, A. Danciu, and A. M. Barrio, "A RST design approach for the launchers flight control system," in *Proc. 6th Int. Conf. Aerodynamics Tools Techn.*, 2016, pp. 32–37.
[70] Z. A. Ali, D. Wang, S. Masroor, and M. S. Loya, "Attitude and altitude control of trirotor UAV by using adaptive hybrid controller," *J. Control Sci. Eng.*, vol. 2016, pp. 1–12, Jun. 2016.
[71] C. Sandu, D. Popescu, and C. Dimon, "Polynomial RST control for blood pressure regulation," in *Proc. 20th Int. Conf. Control Syst. Comput. Sci.*, May 2015, pp. 65–70.
[72] A. Jacknoon, M. Hassan, and S. E. Ferik, "Design of RST controllers based on intelligent optimization algorithms," in *Proc. Conf. Basic Sci. Eng. Stud. (SGCAC)*, Feb. 2016, pp. 177–182.
[73] A. Elmansouri, J. El mhamdi, and A. Boualouch, "Wind energy conversion system using DFIG controlled by back-stepping and RST controller," in *Proc. Int. Conf. Electr. Inf. Technol. (ICEIT)*, May 2016, pp. 312–318.
[74] M. A. F. Lima, J. O. Trierweiler, and M. Farenzena, "A new approach to estimate the minimum variance control law for nonminimum phase multivariable systems," *IFAC-PapersOnLine*, vol. 52, no. 1, pp. 886–891, 2019.
[75] B. Ozyurt, F. Soysal, Z. Y. Hitit, S. Camcioglu, B. Akay, and S. Ertunc, "An efficient dark fermentative hydrogen production by GMV control of pH," *Int. J. Hydrogen Energy*, vol. 44, no. 36, pp. 19709–19718, Jul. 2019.
[76] Z. Zhang and J. Chen, "Enhancing performance of generalized minimum variance control via dynamic data reconciliation," *J. Franklin Inst.*, vol. 356, no. 15, pp. 8829–8854, Oct. 2019.
[77] D. W. Clarke and P. J. Gawthrop, "Self-tuning controller," *Proc. Inst. Electr. Engineers*, vol. 122, no. 9, pp. 929–934, 1975.
[78] K. J. Astrom and B. Wittenmark, "On self-tuning regulators," *IFAC Automatica*, vol. 9, no. 2, pp. 185–199, 1973.
[79] A. S. Silveira, J. E. N. Rodríguez, and A. A. R. Coelho, "Robust design of a 2-DOF GMV controller: A direct self-tuning and fuzzy scheduling approach," *ISA Trans.*, vol. 51, no. 1, pp. 13–21, Jan. 2012.
[80] R. D. B. Araujo and A. A. R. Coelho, "Filtered predictive control design using multi-objective optimization based on genetic algorithm for handling offset in chemical processes," *Chem. Eng. Res. Design*, vol. 117, pp. 265–273, Jan. 2017.
[81] T. C. F. Pinheiro and A. S. Silveira, "Constrained discrete model predictive control of an arm-manipulator using Laguerre function," *Optim. Control Appl. Meth.*, vol. 1, pp. 1–20, Aug. 2020.
[82] K. Ogata, *Modern Control Engineering*. Upper Saddle River, NJ, USA: Prentice-Hall, 1970.
[83] J. Corriou, *Process Control: Theory and Applications*, 2nd ed. Cham, Switzerland: Springer, 2018.
[84] E. Bini and G. M. Buttazzo, "The optimal sampling pattern for linear control systems," *IEEE Trans. Autom. Control*, vol. 59, no. 1, pp. 78–90, Jan. 2014.
[85] M. S. Fadali and A. Visioli, *Digital Control Engineering: Analysis and Design*, 3rd ed. New York, NY, USA: Academic, 2019.

MARYSON DA SILVA ARAÚJO was born in São Francisco do Pará, Brazil, in 1983. He received the B.S. and M.S. degrees in electrical engineering from the Federal University of Pará (UFPA), Belém, Brazil, in 2009 and 2011, respectively, where he is currently pursuing the Ph.D. degree in electrical engineering with the Control and Systems Laboratory (LACOS).

From 2012 to 2013, he was a third Engineer Officer with Transpetro, an affiliate from PETROBRAS. He is also a Researcher with LACOS, UFPA, and an Adjunct Professor with the Engine Teaching Division, Almirante Bráz de Aguiar Instruction Center (CIABA), Brazilian Navy. He is the author of one book, two book chapters, some didactic materials, and some papers. His research interests include automation, digital control systems, refrigeration systems, power systems, systems identification, and transforms applied to control and power systems.

ANTONIO DA SILVA SILVEIRA received the Ph.D. degree in automation and systems engineering from the Federal University of Santa Catarina (UFSC), in 2012. He is currently an Adjunct Professor with the Institute of Technology, Federal University of Pará (UFPA), working on undergraduate and graduate courses in the areas of control and systems in electrical and biomedical engineering.